

Using Physiography as a Lens to Understand Stream Network Expansion and Contraction Across Spatiotemporal Scales

Delaney M. Peterson¹, C. Nathan Jones¹, Kaci Zarek^{1,2}, Michelle Wolford¹, Chelsea R. Smith¹, Charles T. Bond³, Stephen Plont¹, Maggi Kraft⁴, Shannon Speir⁵, Sam Zipper^{6,7}, Sarah E. Godsey⁴, Jonathan P. Benstead¹, Ariel J. Shogren¹, Kevin A. Kuehn³, and Carla L. Atkinson¹

¹Department of Biological Sciences, University of Alabama, Tuscaloosa, AL, USA.

²Department of Ecology and Evolutionary Biology, Cornell University, Ithaca, NY, USA.

³School of Biological, Environmental, and Earth Sciences, University of Southern Mississippi, Hattiesburg, MS, USA.

⁴Department of Geosciences, Idaho State University, Pocatello, ID, USA.

⁵Department of Crop, Soil, and Environmental Sciences, University of Arkansas, Fayetteville, AR, USA.

⁶Kansas Geological Survey, Lawrence, KS, USA.

⁷Department of Geology, University of Kansas, Lawrence, KS, USA.

Corresponding author: Delaney Peterson (dmpeterson2@crimson.ua.edu)

This is a non-peer-reviewed manuscript being submitted to Water Resources Research.

Key Points:

- Contrary to existing perceptual models, stream network expansion/contraction patterns in low-relief watersheds are not driven by topography.
- We found that considering topographic, geologic, and vegetative drivers together best explained the variability observed in our watersheds.
- Sensor placement matters: expanding the sensor network to hydrologically variable reaches increased significance of topographic drivers.

Abstract

Non-perennial streams (i.e., streams that cease flowing regularly across time or space) comprise 60% of the global river network and play an important role in the physical, chemical, and biological functions of downstream waters. However, predicting the dynamic spatiotemporal patterns of network expansion and contraction remains a key challenge across regulatory, practitioner, and research communities, especially given that most investigations focus on high-relief watersheds. To address this challenge, here we employed physiography as a lens to investigate the impacts of geology, soil characteristics, topography, and vegetation on spatial and temporal patterns of stream network expansion and contraction. We instrumented three low-relief headwater networks spanning the Coastal Plain, Piedmont, and Appalachian Plateaus physiographic provinces in the southeastern United States. In each network, we utilized ≥ 20 water presence/absence sensors across two water-years (2023 and 2024) to investigate seasonal and interannual variability in network extent. Network expansion and contraction was driven by a combination of physiographic variables, and existing topography-based methods of predicting network expansion and contraction performed poorly. Our results also emphasize the role that sensor placement plays in understanding network-scale patterns, as deploying sensors in areas of greatest hydrologic variability better captured the full range of network expansion and contraction. This study demonstrates that low-relief stream networks do not conform to existing topography-based perceptual models of network expansion and contraction, and that consideration of other factors such as soils and vegetation are required to explain network expansion and contraction in these ubiquitous landscapes.

Plain Language Summary

Streams that stop flowing somewhere across space or time make up large portions of river systems and play important roles in water quantity and quality of larger rivers. However, it is still difficult to predict where and how stream network length changes through time, as previous work has mainly focused on measuring flowing stream length in mountainous watersheds. This makes it challenging to effectively regulate, manage, and research stream networks, particularly in less mountainous regions. To address this challenge, we investigated stream network length across time and space using the lens of physiography, or the topography, geology, soil, and plant community structure of landscapes. We placed 20 sensors that measured water presence in three

watersheds to understand network length throughout seasons and between years. We found that network length in our three gently sloping watersheds was influenced by variables from all components of physiography, rather than just topography as other studies have suggested. We also found that the location of the sensors influenced patterns in observable stream length. Altogether, this study demonstrates the importance of considering systems with little elevation change, as well as drivers other than topography, to better predict how the length of stream networks changes through time.

1 Introduction

Streams are inherently dynamic features on the landscape (Godsey & Kirchner, 2014), as their response to inputs from precipitation and subsurface storage zones can manifest as extreme streamflow variation at daily to decadal scales. Non-perennial streams are portions of the stream network that cease flowing regularly across either space or time (Busch et al., 2020), often in headwater segments of the network that expand and contract dynamically. Non-perennial streams constitute at least 60% of global river networks (Messenger et al., 2021) and have important impacts on their downstream reaches (Brinkerhoff et al., 2024; Zimmer et al., 2022) by providing diverse and unique habitat (e.g., Datry et al., 2018), generating unique biogeochemical signals (e.g., Gómez-Gener et al., 2021; Zarek et al., 2025), and contributing to seasonal flow and groundwater recharge (e.g., Zimmer & McGlynn, 2017). However, our understanding of the patterns of longitudinal network expansion and contraction and the processes they control has been biased towards quantifying patterns in streamflow variability related to the watershed outlet, rather than patterns in network extent variability (but see Botter & Durighetto, 2020; Godsey & Kirchner, 2014; Prancevic et al., 2025; Prancevic & Kirchner, 2019). Therefore, identifying the primary drivers of variability in network length across systems is required to predict how non-perennial streams drive spatiotemporal variation in large-scale network connectivity.

Watershed characteristics exert strong control over hydrologic processes and network extent. Many studies have documented how meteorology, geology, and land cover act as first-order controls on streamflow and network expansion and contraction across river systems (e.g., Costigan et al., 2016; Hammond et al., 2021; Hynes, 1975; Zipper et al., 2021). Additionally, recent investigations on controls of network expansion and contraction have investigated the role

of watershed topography, suggesting that flow convergence and valley transmissivity drive patterns in network expansion and contraction by regulating both the volume of subsurface storage and rate of down-valley flow (Godsey & Kirchner, 2014; Prancevic & Kirchner, 2019). However, other studies have found that finer-scale watershed heterogeneity in soil properties (e.g., Gutiérrez-Jurado et al., 2019; Warix et al., 2023) or riparian vegetation (e.g., Newcomb & Godsey, 2023) exert stronger controls on network extent dynamics than topography. Therefore, a clear picture of the hierarchical drivers on flowing network extent is lacking.

Much of our understanding of hydrologic processes and network expansion and contraction is also biased toward high-relief systems, often at low temporal resolution, making prediction difficult in lower-relief systems. Generally, a majority of hydrologic research has been conducted in montane, temperate, high-rainfall watersheds (Burt & McDonnell, 2015; McMillan et al., 2023). For example, Prancevic & Kirchner (2019) synthesized the role that watershed topography played in network extent and stability across 17 watersheds (hereafter, topographic perceptual models). However, the watersheds used in that study were high-relief (i.e., an average watershed relief of 700 m) and not representative of the larger distribution of watershed topography observed across the US (Prancevic et al., 2025). Many other network studies have also been conducted in high-relief locations (e.g., Botter et al., 2024; Ward et al., 2018) or even in synthetic watersheds (e.g., Botter & Durighetto, 2020; Zanetti et al., 2024), with the majority of these studies relying on low temporal resolution network surveys (e.g., Zimmer & McGlynn, 2018) rather than higher temporal resolution sensor networks (e.g., Jensen et al., 2019). Further, while there is no universal sensor deployment strategy, much of our understanding of effective sensor placement has also been developed in high-relief systems (e.g., Dohman et al., 2021; Kindred, 2022; Warix et al., 2023). As a result, we are not able to predict network expansion and contraction reliably in low-relief landscapes, as using currently available topographically-derived relationships involves extrapolation outside of the dataset from which they were generated (Prancevic et al., 2025). This highlights the need to understand the drivers of expansion and contraction dynamics across more diverse physiographic settings.

Physiography provides a framework for understanding these hierarchical interactions and is generally defined as the geologic, topographic, and biotic features of the landscape (Fenneman, 1938), thereby integrating multiple potential hierarchical drivers of network expansion and contraction to provide a more holistic view of the watershed setting. Physiography

has been one of the primary tools that has been operationalized by researchers and managers to classify the physical templates of landscapes, and its hierarchical nature lends itself well to studies at a variety of scales. In the US, Fenneman and others (1938) classified the entire country into physiographic provinces, sections, and districts based on existing records of soils, geology, and resulting vegetative communities. The physiographic provinces (e.g., Coastal Plain) are the coarsest resolution and were originally defined based on broad geomorphic characteristics to identify relatively similar regions across large spatial scales (Fenneman 1938). Subordinate sections (e.g., East Gulf Coastal Plain) and smaller districts (e.g., Fall Line Hills) were based on the same characteristics, but at increasingly higher resolutions to identify similar regions at more localized scales. Therefore, physiography provides a consistent and useful template for conducting hydrologic studies, as watersheds located in the same physiographic provinces should have comparable physical watershed characteristics.

To quantify the effects of physiography on network expansion and contraction, we focus on hydrologic connectivity, broadly defined as the water-mediated movement of materials, organisms, and energy (Jones et al., 2019; Pringle, 2001; Rinderer et al., 2018). Hydrologic connectivity incorporates flows across vertical, lateral, and longitudinal dimensions, as well as through time (Harvey & Gooseff, 2015; Ward, 1989; Zimmer & McGlynn, 2018). Hydrologic connectivity provides a unifying framework for evaluating water fluxes across spatiotemporal scales as well as disciplines (Jones et al., 2019). Here, we focus on network connectivity in the longitudinal dimension at the watershed scale, and define this connectivity as network expansion, contraction, and fragmentation through time. While many studies have paired longitudinal connectivity with observations of discharge at the outlet to investigate the impacts of flow and network variability (e.g., biogeochemical fluxes; Zarek et al., 2025; Zimmer & McGlynn, 2018), fewer studies have focused on the dynamics of longitudinal connectivity as an integrator of within-watershed hydrologic processes.

In this study, our goal was to investigate the interactions between stream network expansion/contraction and watershed characteristics using physiography as a template to understand network extent dynamics. In the southeastern US, a natural physiographic gradient forms as the Appalachian mountains grade into coastal regions. Further, this gradient is complemented by a generally uniform climate; much of the southeastern US receives similar precipitation inputs regardless of physiographic region. Therefore, to test potential drivers of

network connectivity, we instrumented three watersheds across this physiographic gradient as a natural experiment – one in the Coastal Plain, one in the Piedmont, and one in the Appalachian Plateaus. While this gradient spans from the mountains to the coast, we stress that these watersheds are all low-relief relative to other studies (i.e., here, less than 350 m of relief compared to an average of 700 m in Prancevic et al., 2019). We deployed a standardized network of water presence/absence sensors in each watershed, and used these to monitor site- and network-scale flow dynamics across two water-years of contrasting dryness (2023 and 2024). We used this sensor network to address our research objectives: (i) investigate the efficacy of existing topographic perceptual models for predicting network expansion and contraction, (ii) characterize the spatial and temporal patterns and drivers of network connectivity and water persistence across an understudied, relatively low-relief region, and (iii) interrogate the role that sensor placement plays in network-scale metrics of connectivity.

2 Methods

2.1 Site Descriptions

We instrumented three watersheds across a physiographic gradient in Alabama (US; Figure 1A). Each watershed was selected to represent the general watershed structure of its larger physiographic province, while also containing non-perennial, headwater portions of the larger stream network. Our watersheds were small and generally similar in size, and we used a standardized site design to maximize comparability between networks (see Section 2.2.1). Further, all three watersheds had a humid subtropical climate, with a mean annual precipitation ranging from 1,350 to 1,400 mm per year, and mean annual temperatures ranging from 15.3 to 17.8°C (NOAA NCEI, 2025). We describe each research watershed below and outline their key components in Table 1. However, there is considerable heterogeneity across headwater watersheds (Golden et al., 2025), and while the gradients observed across our watersheds likely reflect broader regional differences, within-watershed observations probably do not capture the full range of conditions present throughout each region. Additional information can be found in the Detailed Site Descriptions in *Text S1*.

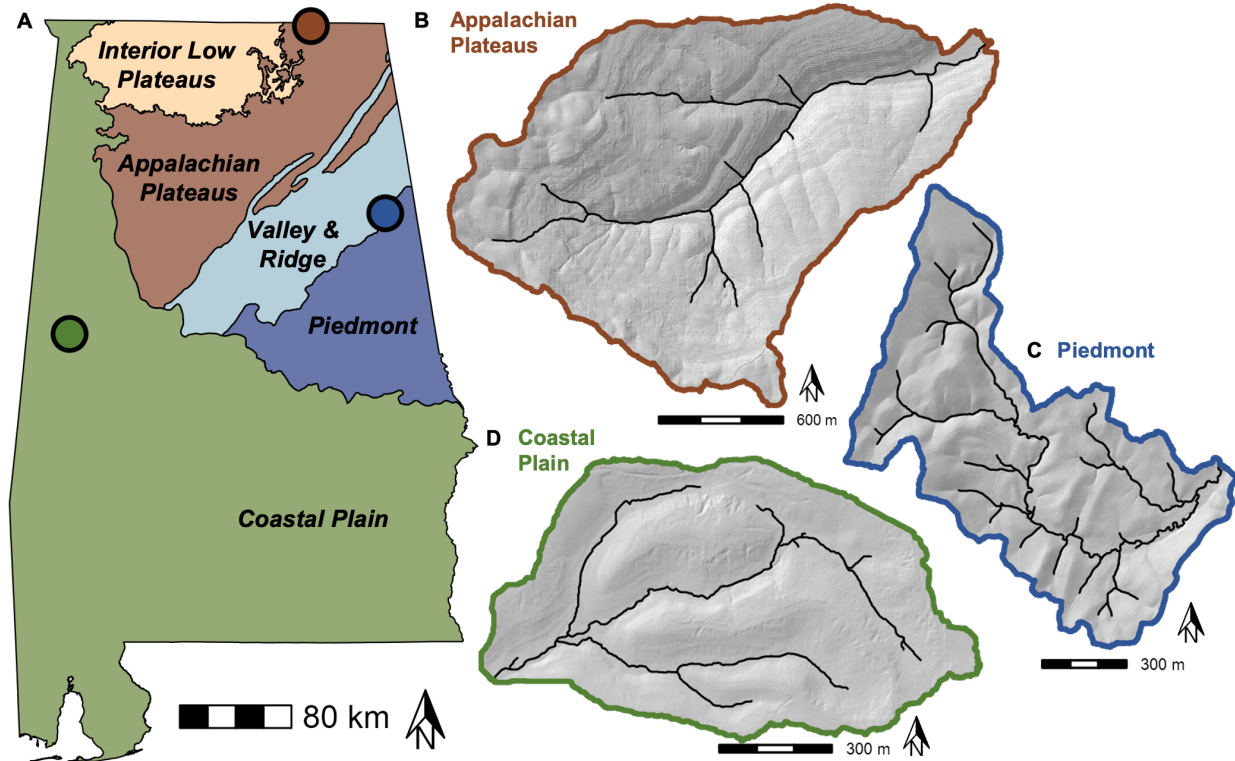


Figure 1. (A) A map of Alabama, US colored by physiographic provinces. Each point corresponds to one of the three research watersheds, (B-D) which are also colored by physiographic province. (B-D) Hillshade maps of the three research watersheds, with the geomorphic channel network mapped by the black lines.

Table 1. *Watershed Characteristics*

Research watershed	Outlet location (Lat., Lon.)	Mean Jan. temp. [°C] ^a	Mean Jul. temp. [°C] ^a	Mean annual precip. (mm/yr) ^a	Elevation range (relief, masl)	Watershed area (km ²)	Average (min., max.) Slope (%)	Primary lithology	Primary soil texture ^b
Appalachian Plateaus	34.968617, -86.165017	4.4°	25.4°	1,390	211 - 550 (339)	2.97	17 % (0.01, 69)	Karstic sedimentary	Silty clay loam
Piedmont	33.762197, -85.595507	5.3°	25.3°	1,400	345 - 456 (111)	0.92	12 % (0.005, 49)	Low-grade fractured metamorphic	Silt loam
Coastal Plain	32.984109, -88.013343	7.3°	27.4°	1,350	63 - 94 (31)	0.70	7 % (0.001, 28)	Sedimentary marine deposits	Fine, sometimes sandy, loam

^aObtained from NOAA NCEI (2025).

^bObtained from Soil Survey Staff (2025).

2.1.1 Appalachian Plateaus research watershed

Our watershed in the Appalachian Plateaus province drains a non-perennial tributary of Burks Creek in Jackson County, AL (US; Figure 1B). During the study period, the 2023 water year had 1,350 mm of precipitation, and the 2024 water year had 1,300 mm (Table 1). While precipitation was below average during the study period, the previous water year (2022) had above-average precipitation of 1,540 mm. This watershed has the highest relief of our three study sites, and is underlain by karstic Missippian-age sedimentary lithologic units (Table 1). In the headwaters, there are abundant cave-springs at the exposure of the Bangor limestone unit, as well as spring discharges from numerous fractures (Ponta, 2018). There is little soil development within this watershed, primarily as a function of the steep stony slopes and geologic erosion (Swenson, 1954). The upper portions of the watershed have thin, organic soils primarily in the Mollisol soil order, and the streambeds are primarily exposed bedrock benches. Conversely, the soils in the lower portions of the watershed are highly weathered Ultisols, and stream sediment aggradation occurs in the lower portion of the network (Soil Survey Staff, 2025). This watershed is almost entirely forested with primarily deciduous species, and is privately owned and managed for hunting and conservation. This watershed, like much of the area, was used for silvicultural harvest until around the turn of the 20th century, resulting in a mixed-age forest (Swenson, 1954). Additionally, portions of the valley bottom and several areas in the headwaters have been cleared for cultivation, but the majority of the riparian zone is forested.

2.1.2 Piedmont research watershed

Our watershed in the Piedmont province drains a non-perennial tributary to Pendergrass Creek in Cleburne County, AL (US, Figure 1C). During the study period, the 2023 water year had 1,400 mm of precipitation, and the 2024 water year had 1,390 mm (Table 1). This network drains our moderate-relief watershed, and is underlain by Silurian-Devonian-age low-grade metamorphic lithologic units that have formed highly weathered soils (Table 1). The groundwater systems in this region are highly complex due to the fractured lithology, but the primary lithologic unit in this watershed is included in the metasedimentary and metavolcanic aquifer system, which is an unconfined water-table aquifer (Kopaska-Merkel et al., 2000). This watershed is dominated by highly weathered Ultisols. The upper portions of the watershed have

thin and rocky soils where the regolith is closer to the surface (Feminella, 1996; Kopaska-Merkel et al., 2000), with primarily coarse stream sediments (i.e., gravel, pebbles, and cobbles). Conversely, the lower portion of the watershed has more developed, argillic soils, and the streambeds consist of a mix of coarse and finer-grained (i.e., sand, silt) sediments (Zarek et al., 2025). This watershed is entirely forested with mixed deciduous and coniferous species within the federally-owned Talladega National Forest, and is managed for recreation, silviculture, and conservation.

2.1.3 Coastal Plain research watershed

Our watershed in the Coastal Plain province drains a non-perennial tributary to Shambley Creek in Greene County, AL (US; Figure 1D). During the study period, the 2023 water year had 1,450 mm of precipitation, and the 2024 water year had 1,250 mm (Table 1). This watershed has the lowest relief in our study, and is underlain by Upper Cretaceous-age sedimentary lithologic units that are primarily sand and clay that have formed highly weathered soils (Table 1). The watershed is dominated by highly weathered Ultisols, Alfisols with argillic horizons, and poorly organized Entisols (Soil Survey Staff, 2025). The stream substrate of this watershed are primarily fine-grained sediments (i.e., clay lenses, silt, sand), with some conglomerate pebbles near the watershed outlet. Further, the combination of highly erodible soils and low relief has resulted in highly incised portions of the network, with over half (55%) of the network incised > 0.5 m below the riparian zone, and some areas of incision nearly 2 m deep. This watershed is entirely forested with mixed coniferous and deciduous species, privately owned by the Weyerhaeuser Company, and managed for rotational silvicultural harvest. Within this watershed, the uplands are almost entirely pine species, with dense, primarily oak riparian vegetation. The southern upland portion of the watershed was thinned and harvested in the summer of 2024, but all forest within 11 m of the stream channel was preserved.

2.1.4 Within-watershed Hydrogeomorphic Features (HGFs)

To characterize the inherent variability of river corridor structure within our watersheds, we further delineated each watershed into distinct units linked to their hydrologic functions known as hydrogeomorphic features (HGFs), following Peterson et al. (2024). Each HGF was assigned based on key structures across the river corridor that we identified in the field as

potential regulators of hydrologic connectivity. Notably, these HGFs integrate topographic, geologic, and vegetative characteristics across the entire river corridor (i.e., the stream channel and adjacent riparian zones and hillslopes). In the Appalachian Plateaus, we delineated the network into two HGFs: (i) bedrock channels and (ii) alluvial channels. Bedrock channels dominated the upstream half of the watershed, and were defined by exposed bedrock streambeds with little substrate accumulation and steep slopes, while the alluvial channels were defined as lower-gradient channels with finer substrates and sediment accumulation (*Figure S1*). In the Piedmont, we delineated the network into three similar units: (i) headwaters, (ii) transitional channels, and (iii) valley-bottom channels. Headwaters were defined as the highest portions of the network that also had highly constrained valleys and steep slopes; transitional channels had wider valleys and approximately 0.5 m of channel incision; and valley-bottom channels had wide and dense riparian zones with low slopes and meandering channels (*Figure S2*). In the Coastal Plain, where the HGF concept was developed in Peterson et al. (2024), we delineated the network into three units: (i) wetland-stream complexes, (ii) intact riparian zones, and (iii) incised channels. Wetland-stream complexes were defined as low-gradient reaches with high width-depth ratios; intact riparian zones were defined as channels with distinct banks and evidence of out-of-bank flows into the riparian zone; and incised channels were defined as deeply entrenched (> 0.5 m of incision) channels that had lost access to the riparian zone (*Figure S3*).

2.2 Hydrologic Monitoring Instrumentation

To quantify network length across time, as well as water persistence at each site, we instrumented each watershed with at least 20 water presence/absence sensors, as well as a discharge monitoring station at each network outlet. All instrumentation collected continuous data for the two-year study period. All sensors logged at concurrent 15-minute intervals from 1 Oct. 2022 through the spring of 2024, and then logged at concurrent hourly intervals from the spring of 2024 through Sep. 2024.

2.2.1 Watershed-Scale Network Length Monitoring

Each watershed was instrumented with at least 20 water presence/absence, or Stream Temperature, Intermittency, and Conductivity (STIC) sensors (*sensu* Chapin et al., 2014; Jensen et al., 2019). To maximize comparability across networks, we used a standardized site selection

design based on the relationship between contributing area and topographic wetness index (outlined in Swenson et al., 2024; Zipper et al., 2025). This resulted in sensor networks that targeted a gradient of wetness conditions, rather than a uniform density. For an 11-month period (May 2022 through April 2023), we deployed an additional 29 STICs in the Piedmont watershed to capture a higher resolution and density of conditions across the watershed in coordination with a large synoptic sampling effort (June 2022). These sensors were placed strategically to fill spatial gaps in the existing network, while also expanding up into the upstream tips of the geomorphic network.

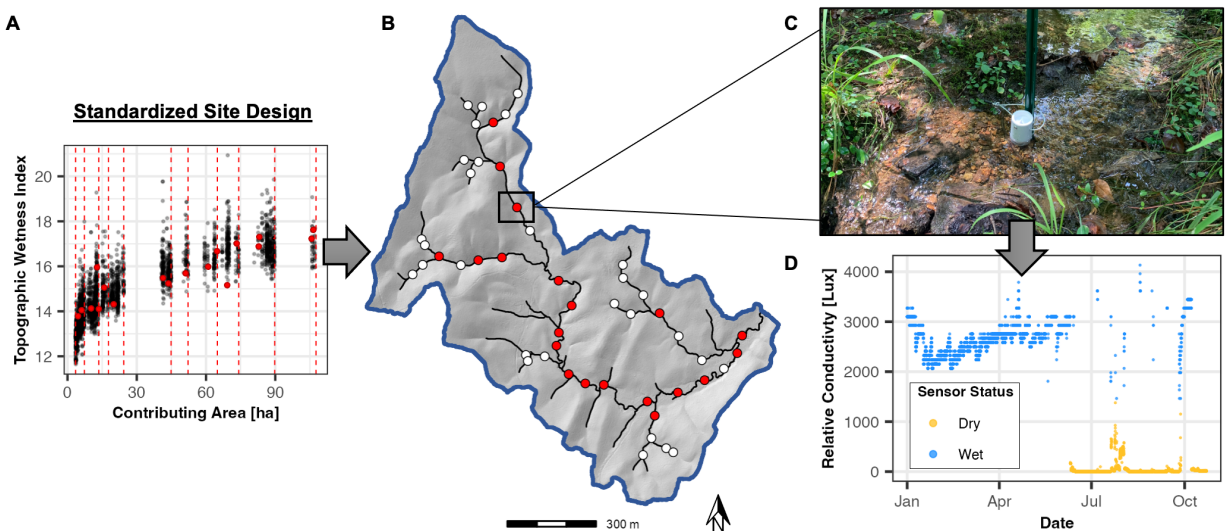


Figure 2. Standardized site design for sensor placement within each watershed network. **(A)** The distribution of cells within the watershed raster, binned by contributing area. Selected points are indicated in red. **(B)** The Piedmont watershed, with the selected site locations indicated in red. The additional 29 strategic locations are indicated in white. **(C)** An image of a STIC deployed in a field reach. **(D)** An example output from the STIC, with relative conductivity (in units of Lux due to legacy sensor modification) across time, and the water presence/absence indicated by the color of each point. See *Figure S4* for sensor placement in the Appalachian Plateaus and Coastal Plain sites.

At each site, we placed STIC sensors in the thalweg at the highest point (i.e., the head of a riffle) within the reach selected by the standardized site design to collect both temperature and relative conductivity at regular, concurrent intervals. This allowed sensors to detect stream connectivity when wet and stream fragmentation when dry. Sensors were anchored within 1 cm

of the stream bed to capture low flows. We maintained and downloaded data from the sensors every 4-6 months, and removed the sensors for 3-7 days to change the batteries every 9 months. During every maintenance visit, we also recorded water presence/absence at the site and height of the sensor relative to the streambed to validate sensor measurements. Sensors were deployed from September 2021 to October 2024; however, we used the data from all permanent sensors from October 1, 2022 through September 30, 2024 for this study.

We used a project-specific data-processing pipeline to clean and quality-control STIC sensor data (Zipper et al., 2025). Briefly, we converted the uncalibrated relative conductivity to a binary wet/dry metric based on sensor-specific thresholds identified via laboratory calibrations prior to deployment (i.e., 0 uS/cm as a minimum possible wet reading; Burke et al., 2024; S. Godsey et al., 2024). We then quality-controlled all data following Zipper et al. (2025). Finally, we filtered all data to periods of time where all sensors were recording concurrently to build our final dataset. We then used the GPS locations of each sensor to calculate a representative reach length as the sum of half the distance from the downstream and upstream sensors, such that the reach was centered around the sensor of interest and accounted for branches and tributaries. We used these sensor measurements to calculate the length of the active surface drainage network (hereafter, ASDN in m, *sensu* Zimmer & McGlynn, 2018) as the total length of the wet stream network. Here, we calculated ASDN length at continuous and daily timesteps by summing reach lengths for all wet sensors. Additionally, for each individual sensor, we calculated the local water persistence as the number of wet observations across the period of record divided by the total number of observations. Notably, streambeds in the southeastern US are highly mobile, and streambed erosion and deposition imply that some of our sensor locations likely did not always remain the first to dry throughout the study as they were initially installed. Therefore, our assumption that each sensor represents its neighboring 100-500 m reach might not be accurate at every time point in this study.

2.2.2 Watershed Outlet Discharge Monitoring

At the outlet of each watershed, we installed high-frequency monitoring stations that measured stream water level (meters) at the same 15-minute intervals, as well as a suite of other measurements (for more information, see section 2.3 of Zarek et al., 2025). The stream

monitoring well was instrumented with a Seametrics PT12 pressure sensor that recorded relative stream water level from September 2021 onwards. In each watershed, this sensor was eventually replaced by an Onset HOBO U20L pressure transducer (Piedmont in January 2023, Coastal Plain in June 2023, and Appalachian Plateaus in June 2024). We converted the instantaneous level measurements to absolute elevation (meters above sea level, hereafter masl) using channel geometry surveys and a co-located HOBO U20L pressure transducer to collect barometric pressure, and paired them with rating curves developed using salt dilution-gauging discharge measurements to develop a continuous record of instantaneous discharge (in L/s) at each watershed outlet for the study period.

2.3 Physiographic Analyses

To contextualize our network results, we calculated a suite of topographic, geospatial, and vegetative metrics to characterize the physiography of the three watersheds (see *Table S1*). Using publicly available data (i.e., DEMs from USGS, geology and soils data from NRCS) as well as geomorphometric tools from the *whitebox* package in R (Wu & Brown, 2022), we calculated topographic, geologic, and pedologic metrics at both the site- and HGF-scales. Additionally, we used field data collected in tandem with this work to calculate vegetative metrics at the HGF-scale. We paired these metrics with our network analyses (e.g., drainage density, curvature, and slope coefficients; Table 2) to interrogate the physiographic drivers of stream connectivity. All analyses were performed using R v4.4.0 (R Core Team, 2023).

2.3.1 Topographic Analysis

First, we obtained high-resolution (1-m or finer) DEMs for each of our watersheds from the USGS national map downloader v2.0 (<https://apps.nationalmap.gov/downloader/>). We processed these DEMs by filtering, filling pits, and breaching depressions using the respective *whitebox* functions in R version v.4.4.0 (R Core Team, 2024; Wu & Brown, 2022). We then used the *wbt_watershed()* function to delineate our watersheds, and used the d8 flow direction and flow accumulation rasters to delineate our stream networks. We defined minimum flow accumulation thresholds for each watershed that yielded networks most closely matching the geomorphic channel network (60,000 1-m cells in the Appalachian Plateaus; 10,000 0.92-m cells

in the Piedmont; 12,000 1-m cells in the Coastal Plain). These watersheds and stream networks were then used as the foundation for the rest of the topographic metrics.

We calculated site-specific topographic metrics at each sensor location to compare with our network metrics. We calculated elevation, slope at several scales (see *Table S1*), drainage area, distance to outlet, upstream network length, topographic wetness index (TWI), curvature, and aspect using the respective functions in the *whitebox* package (Wu & Brown, 2022), and topographic position index (TPI) by using the *multiscaleDTM* package (Ilich et al., 2025) to generate rasters of these variables. We then used the sensor location data (snapped to the delineated stream network) to extract the values of these variables for each location. We calculated drainage density as a proxy for topographic convergence by dividing the upstream length by the drainage area for each location. Additionally, we calculated slope in a 5-m buffer zone (buffer slope, *Table S1*) around each sensor by averaging all cells in the buffer to integrate riparian and valley slope conditions near the sensor. We also calculated channel slope by generating a continuous stream slope raster and averaged the slope of all cells from the stream network raster in a 12.5-m buffer that equated to a 25-m stream reach.

To understand the sensitivity of stream network length to changes in flow, as well as the potential topographic controls of that sensitivity, we plotted stream network length as a function of outlet discharge. As this sensitivity has been related to three primary components of watershed topography – flow convergence, changes in gradient, and curvature – we further calculated these factors throughout each network following Prancevic & Kirchner (2019). We assessed the sensitivity of the stream network length as a function of discharge at the watershed outlet, and extracted the slope of the power-law relationship as our network expansion exponent (β). Using the delineated geomorphic channel network, we calculated the drainage density, total curvature, slope, and contributing area for each point along the network. We then calculated the exponents of the power-law relationships between drainage density and channel activation (α), slope and area (θ), and curvature and area (δ) (*sensu* Prancevic & Kirchner, 2019; *Table S1*). Finally, we compared the slope-area and drainage density-channel activation relationships derived from network topography with the expected network expansion exponent, β (as demonstrated in Eqn.

4 in Prancevic & Kirchner, 2019) to assess whether local topographic controls on network expansion and contraction aligned with global patterns observed in high-relief watersheds.

2.3.2 Geospatial Analysis

We gathered additional geospatial data to further contextualize our results using geologic and soils data from the NRCS Web Soil Survey. First, we used the Web Soil Survey to extract the primary soil map units within our watersheds (Soil Survey Staff, 2025). We then extracted depth to bedrock, saturated hydraulic conductivity, percentages of each soil texture class, organic matter content in the surficial 50 cm, and primary lithologic underlying units from each soil map unit (*Table S1*). We also used the soil maps within each watershed to extract these variables for each sensor location. We then aggregated these variables by HGF to evaluate relationships between these patterns at a more appropriate scale, as the Web Soil Survey was developed at a coarser resolution.

2.3.3 Vegetation Analysis

We derived relative proportions of vegetation types from densiometer measurements taken throughout the watershed across seasons. In short, densiometer measurements were taken at seven locations within each watershed at least four times throughout the two-year study period. Additional densiometer measurements were taken at all 49 sensor locations in the Piedmont research watershed once in June 2022. Each individual measurement consisted of averaging four to six canopy cover measurements within the study reach, and canopy cover was calculated as the total number of covered quadrants within the densiometer divided by the total number of quadrants.

Using both these temporally and spatially distributed measurements, relative proportions of vegetation types were calculated by comparing late-winter leaf-off measurements (i.e., a proxy for coniferous vegetation) to late-summer leaf-on measurements. For each location, the leaf-off measurements were subtracted from their respective leaf-on measurements to calculate relative proportion of deciduous vegetation. These calculations were then aggregated by HGF, and the percent of deciduous vegetation was calculated as the average ratio of deciduous

vegetation to the total leaf-on measurement $\times 100$. The percent of coniferous vegetation for each HGF was calculated as the average ratio of leaf-off measurement to leaf-on measurement $\times 100$.

2.4 Statistical Analyses

To evaluate relationships and statistical significance between physiographic variables and water persistence, we first filtered the dataset to include only non-perennial sensors (i.e., sensors that recorded dry conditions at some point across the study period; $n = 13$ for the Piedmont watershed, $n = 19$ for the Appalachian Plateaus and Coastal Plain watersheds) for the 2024 water year. We selected the 2024 water-year to maximize network contraction, as this was the driest year of the study, when all three watersheds experienced the greatest network contraction and subsequent shortest ASDN lengths. All analyses were performed on this subset of data and were grouped by study watershed unless noted otherwise.

For the relationships between physiographic variables and water persistence, we performed individual correlation tests between each variable and water persistence using Spearman's rank correlation coefficient (ρ) to account for our non-parametric data. For within-watershed statistical testing, we aggregated the sensors into groups according to their HGFs (as noted above in section 2.1). We then used a Kruskal-Wallis test to evaluate significance of each physiographic variable and water persistence across the groups. For significant relationships, we then performed a post hoc Dunn's test to evaluate which differences between pairwise groups were significant. For all statistical analyses, we assigned a significance level of $p < 0.05$.

To test the hierarchical relationship between all of our physiographic variables, we also used a random forest model to evaluate variable importance. We constructed four random forest models – one model for each watershed, as well as one global model using data across all three watersheds – using the *randomForest* package in R (Liaw & Wiener, 2024). For each model we first filtered out highly correlated predictor variables by calculating Spearman's rank correlation coefficient for every pair of potential variables and removing one variable from each pair with $\rho > 0.9$. We split our data into training and testing sets, randomly assigning 70% of our observations to the training set and the other 30% to the testing set. We then used this final predictor variable and training dataset in the model and constructed the final model using 500 trees and 5 predictor variables at a time. We evaluated model performance by calculating Root

Mean Squared Error (RMSE), coefficient of determination (R^2), Mean Absolute Error (MAE), and Mean Absolute Percent Error (MAPE) for both our training and testing datasets. Finally, we evaluated variable importance by calculating the percent increase in Mean Standard Error (incMSE%) for each variable when it was removed from the model.

3 Results

3.1 Topographic metrics are poor predictors of network connectivity in Southeastern US watersheds

We calculated the topographic metrics outlined by Prancevic & Kirchner (2019) to compare the patterns in our watersheds to other well-studied stream networks. We observed that of our three watersheds, the Appalachian Plateaus had the highest coefficients for all three of the topographically derived calculations (*Table S2*). Conversely, the Coastal Plain site had the smallest slope ($\alpha = 0.156$) and drainage density ($\theta = 0.271$) exponents of our three watersheds, but the Piedmont had the smallest curvature coefficient ($\delta = -2.84$; *Table S2*). Further, both the Piedmont and Coastal Plain had negative curvature coefficients. We also used the relationship between curvature and transmissivity to investigate how potential topographic drivers varied both within and across our networks. In most watersheds, curvature increases whereas transmissivity decreases moving down the network. However, this was only observed in one of our watersheds (the Appalachian Plateaus, Figure 3A). Rather, in our Piedmont and Coastal Plain watersheds, curvature decreased along with transmissivity moving down the network (Figure 3A), though for the Coastal Plain, the effect size was negligible and aligned with the general expected relationship between curvature and transmissivity.

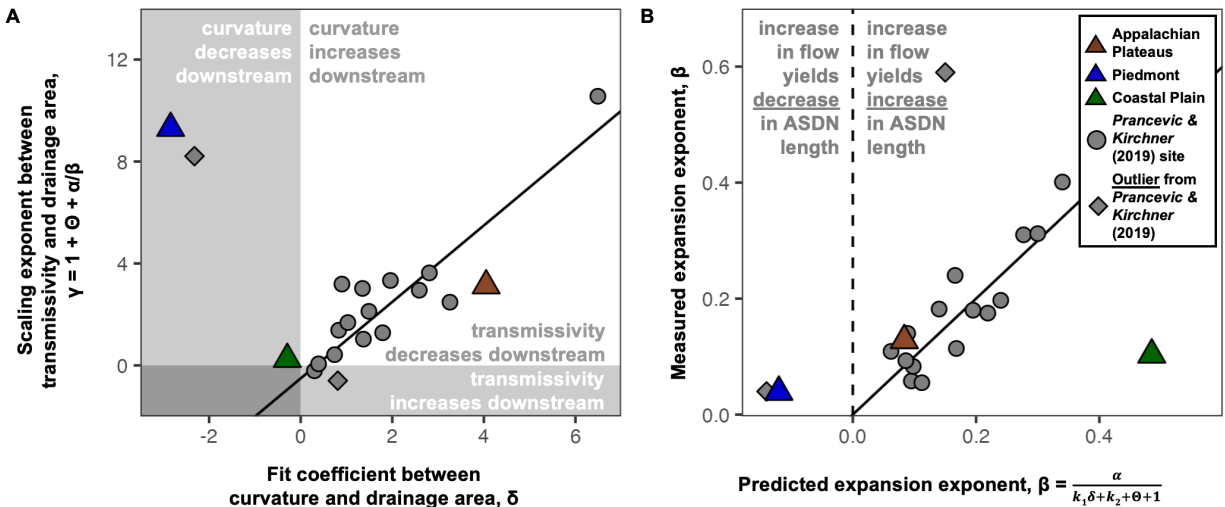


Figure 3. Relationships between curvature and transmissivity (A) and predicted vs. observed expansion exponents (B) following Prancevic & Kirchner (2019). In both panels, grey points correspond to observations from the original 17 watersheds used in Prancevic & Kirchner (2019). Colored triangles correspond to the watersheds in this study. Additionally, the two most distinct outliers from the original 17 watersheds (Coweeta 40 and Hubbard Brook 25) are denoted by diamonds.

Further, we compared the predicted relationship between discharge and network length to the measured relationship (as expansion exponent β ; Prancevic & Kirchner, 2019) to quantify how well topographic patterns explained network connectivity. The Appalachian Plateaus watershed was mostly comparable between the predicted and observed expansion exponent β (0.08 vs 0.13; Figure 3B). However, there was poor agreement between predicted and observed expansion exponent β for the Piedmont and Coastal Plain watersheds. Using the topographic relationships, the Piedmont watershed was predicted to contract slightly at higher flows (-0.12), while our results indicated the network was actually fairly stable (0.04, Figure 3B). Conversely, the Coastal Plain was predicted to be more dynamic than observed (0.49 vs 0.10, Figure 3B). Further, the Piedmont watershed was the only watershed with a negative predicted β ; while it did not contract as predicted, it had the lowest observed β of any watershed in this study (i.e., the most stable network). Similarly, the Coastal Plain watershed had the highest predicted β (i.e., most dynamic network), but it overpredicted the network sensitivity to flow. Altogether, these

results indicate that the topographic relationships derived in Prancevic & Kirchner (2019) performed poorly in our Piedmont and Coastal Plain watersheds.

3.2 Magnitude of network expansion and contraction varies across watersheds

Across our three research watersheds, we observed general seasonal patterns and interannual variability in network expansion and contraction. All three watersheds were more connected with greater ASDN lengths in the winter and early spring (Day of Water Year = 100), and were more contracted with lower ASDN lengths in the late summer and early fall (Day of Water Year = 250; Figure 4). However, the exact timing of the start and peak of the annual dry-down varied by watershed, with the Appalachian Plateaus generally starting to contract and reaching its lowest ASDN length earlier than the other watersheds, and the Piedmont contracting and reaching its lowest ASDN length the latest (Figure 4). Further, the timing of the drydown differed between years for both the Appalachian Plateaus and the Coastal Plain, with the drydown reaching its lowest ASDN length earlier in 2024 for both watersheds (Figure 4A,C). In contrast, there was no difference in timing in the Piedmont watershed, with the network reaching its driest point in late September both years (Day of Water Year = 360; Figure 4B).

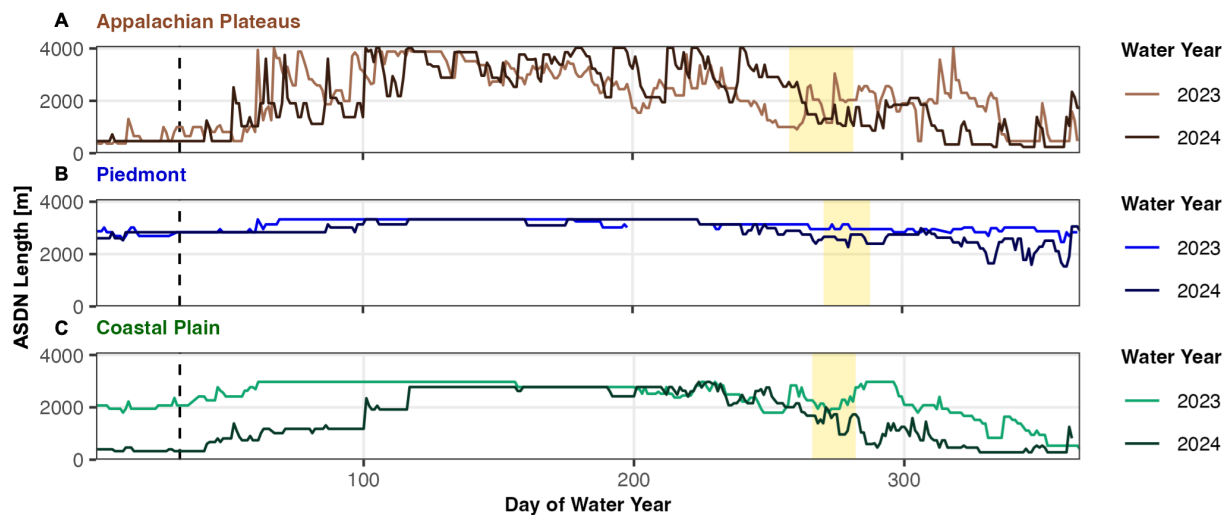


Figure 4. Active Surface Drainage Network (ASDN) length (m) throughout time, with the lighter color reflecting the 2023 water year, and the darker color reflecting the 2024 water year. (A) is the Appalachian Plateaus watershed, (B) is the Piedmont watershed, and (C) is the Coastal Plain watershed. Periods of highest potential evapotranspiration (PET; defined as the 90th

percentile of daily PET values) for each watershed are indicated in yellow, and the start of the leaf-off period is indicated by the vertical dashed line (day of water year = 32).

Further, we observed that the magnitude of network expansion and contraction differed across watersheds. The Appalachian Plateaus watershed had the greatest proportion of network contraction, shrinking from fully connected at 4,026 m in June 2024 to 238 m in August 2024 (100% to 6% of the potential network length; Figure 4A). The Coastal Plain watershed also had a large magnitude of network contraction, going from 2,972 m when fully connected in May 2024 to 282 m in August and September 2024 (100% to 9% of the potential network length; Figure 4C). Comparatively, the Piedmont watershed had very minimal network contraction, only shrinking from fully connected at 3,326 m in May 2024 to 1,417 m in September 2024 (100% to 43% of the potential network length; Figure 4B), suggesting lower sensitivity to interannual climatic variability. Further, the magnitude of network contraction varied between years, with 2024 yielding lower minimum network lengths for all three watersheds. Altogether, we observed that the Appalachian Plateaus and Coastal Plain were relatively dynamic watersheds that went through large cycles of network expansion and contraction, whereas the Piedmont watershed was relatively stable and only saw minimal network contraction.

3.3 Physiographic drivers varied across watersheds

We found that at the watershed scale, topographic metrics were variably important to water persistence across physiographic regions. We compared our 2024 water persistence data for each watershed to three primary topographic drivers: drainage density as a proxy for convergence, slope of the channel network, and curvature (Figure 5). We found that drainage density was significantly and positively related to water persistence for the Coastal Plain watershed ($\rho = 0.52$, $p = 0.03$; Table 2) and for the Piedmont watershed ($\rho = 0.60$, $p = 0.03$; Table 2), where higher flow convergence related to greater water persistence (Figure 5A). We found greater curvature related to higher water persistence in the Coastal Plain (Figure 5C), where there was a positive relationship ($\rho = 0.50$, $p = 0.03$; Table 2). Finally, we found that stream slope was significantly related to water persistence in the Appalachian Plateaus ($\rho = 0.49$, $p = 0.04$) and the Piedmont ($\rho = -0.65$, $p = 0.02$; Table 2); however, the relationship was positive in the Appalachian Plateaus (i.e., steeper slopes related to greater water persistence) but negative

in the Piedmont (i.e., shallower slopes related to greater water persistence; Figure 5B).

Altogether, we found that water persistence in each watershed was significantly correlated to at least one, but not all three, of the primary topographic driver variables. Similarly, we found that no single variable was significantly correlated with water persistence variability in all three watersheds.

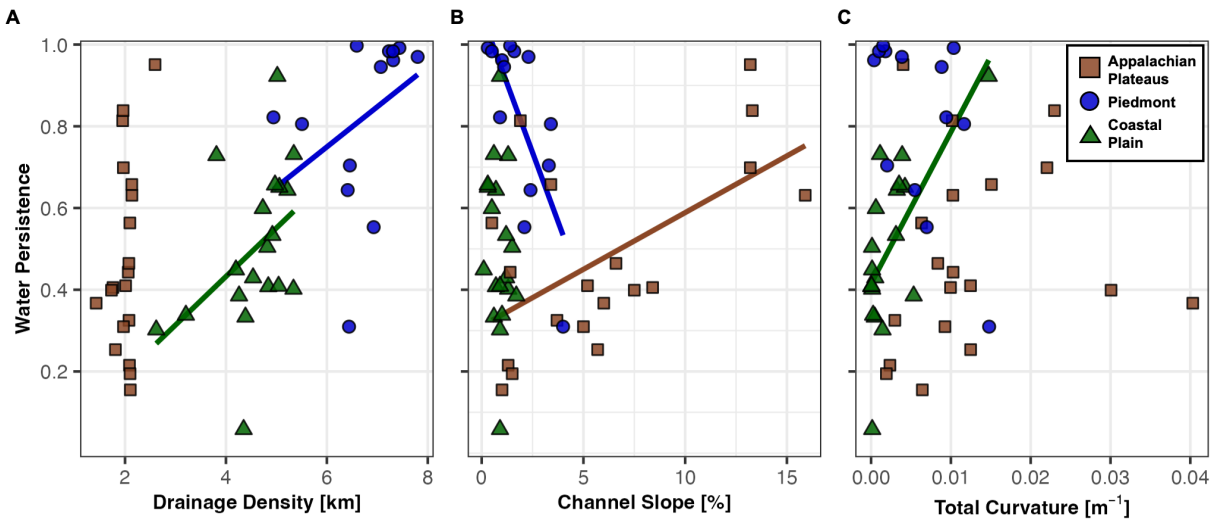


Figure 5. Relationships site-specific water persistence and between the three primary topography metrics: **(A)** flow convergence, **(B)** slope, and **(C)** valley curvature. Relationships with significant correlations (as noted in Table 2) are marked with solid lines. Colored points and lines correspond to the watersheds in this study, where brown is the Appalachian Plateaus, blue is the Piedmont, and green is the Coastal Plain (further indicated in the legend).

Further, we observed that while some topographic metrics were significantly correlated with water persistence for all three watersheds (e.g., TWI; see Table 2), the directionality of these relationships differed between watersheds. For example, the relationship between TWI and water persistence was positive in the Piedmont ($\rho = 0.58$) and Coastal Plain ($\rho = 0.51$), but negative for the Appalachian Plateaus ($\rho = -0.53$). Additionally, we found that several metrics that were significantly correlated with water persistence for each watershed strongly covaried; for example, distance to outlet, drainage area, and TWI are all calculated using the same area accumulation technique, and TWI was significantly correlated with water persistence across all three watersheds. Further, we found that there was a significant relationship between elevation and water persistence for the Piedmont watershed ($\rho = -0.64$, $p = 0.02$), with a negative

relationship (i.e., higher elevations had lower water persistence; Table 2). Altogether, we expect that the relationships observed here likely reflect larger-scale watershed patterns, and thus may correlate with other physiographic drivers.

Table 2. Spearman's Correlation Coefficients (ρ) and Statistical Significance for a Subset of Topographic Metrics

Percent wet ~	Appalachian Plateaus		Piedmont		Coastal Plain	
	ρ	p-value	ρ	p-value	ρ	p-value
Drainage density	0.09	0.72	0.60	0.03	0.52	0.03
Channel Slope	0.49	0.04	-0.65	0.02	-0.25	0.30
Total Curvature	0.32	0.18	-0.48	0.09	0.50	0.03
Elevation	0.41	0.08	-0.64	0.02	-0.39	0.10
Distance to outlet	0.36	0.13	-0.67	0.01	-0.24	0.32
TWI	-0.53	0.02	0.58	0.04	0.51	0.03
TPI	0.09	0.72	0.32	0.28	-0.49	0.04
Buffer slope	0.52	0.02	-0.61	0.03	0.64	< 0.01

Note: All statistics performed on the non-perennial sensors (Piedmont $n = 13$, Appalachian Plateaus and Coastal Plain $n = 19$). Variables in bold are statistically significant.

At the HGF scale, we observed that within-watershed patterns in water persistence were related to watershed physiographic variables (i.e., geologic, vegetative, and soil characteristics, *Table S1*). In the Appalachian Plateaus watershed, the alluvial channels HGF dried 16% more than the headwaters, although this difference was not significant (Figure 6A). Similarly, there were differences between the two HGFs for depth to bedrock ($p = 0.03$; Figure 6D), as well as all other soil and vegetation variables. However, we expect that this is likely an artifact of the structure of our data, as the physical differences between groups were very small, and the data were tightly clustered due to the resolution of the soils map in this region. In the Piedmont watershed, the headwaters were approximately 28% drier than the other two HGFs on average ($p = 0.05$; Figure 6B), but there was no significant difference between the transitional and valley bottom HGFs (though this is likely a function of there being fewer data points in the transitional channels than the other two HGFs). This was also reflected in the other physiographic variables,

where the headwaters had significantly shallower depths to bedrock ($p < 0.01$), higher saturated hydraulic conductivities ($p < 0.01$), and greater percentages of coniferous vegetation ($p < 0.01$; Figure 6E). In the Coastal Plain, the wetland-stream complex and intact riparian zones were approximately 23% drier than the incised channel HGF ($p = 0.03$, Figure 6C), though there was no significant difference between the wetland-stream complexes and the intact riparian zones. Interestingly, there was only a significant relationship between HGF and percentage of coniferous vegetation, where the wetland-stream complex had the highest percentage, and the intact riparian corridor had the least ($p < 0.01$). However, we again expect that this is primarily driven by the structure of the data, as the differences between the values were minimal (less than 10%). Further, there were no significant relationships between soil variables and HGF in the Coastal Plain.

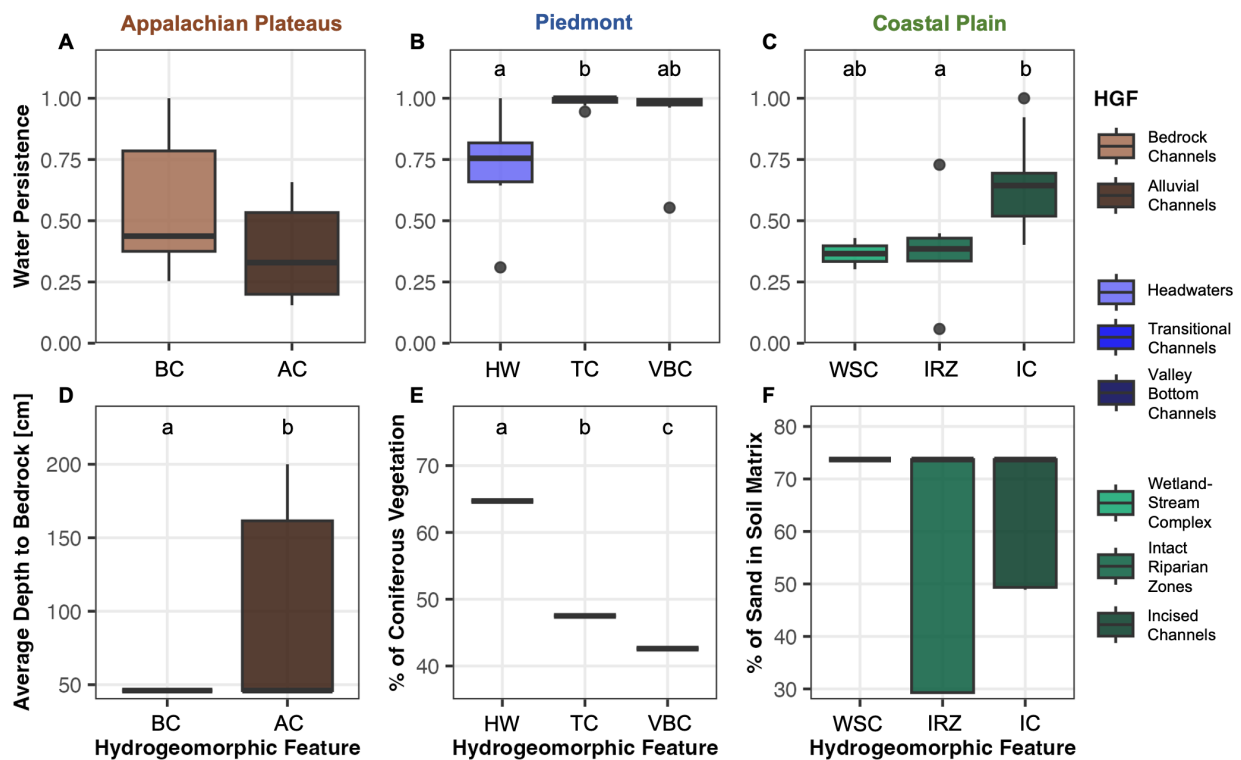


Figure 6. (A-C) Boxplots of water persistence across the HGFs for each watershed. (D-F) Boxplots of different physiographic variables across the HGFs for each watershed. Significance between groups is denoted by letters above each group ($p < 0.05$). Analyses were performed on the entire dataset ($n = 20$ per watershed) for even distribution across groups. HGFs are ordered from most upstream to downstream. Panels (D-F) show variables from different physiographic

categories: **(D)** depth to bedrock as a proxy for geologic features, **(E)** percent coniferous vegetation as a proxy for vegetative community structure, and **(F)** percentage of sand in the soil matrix as a proxy for soil structure. See legends for keys to x-axis labels.

Using random forest models, we observed key differences in the topographic, vegetative, and soil-related drivers of water persistence across our three watersheds. Overall, individual watershed models performed better than the global model (*Table S3*). The Piedmont model was the most robust when evaluating our testing data ($R^2 = 0.75$) with minimal error (RMSE = 0.15, MAPE = 18.5; *Table S3*). The Coastal Plain model also performed well ($R^2 = 0.56$) with the lowest overall error parameters (*Table S3*). In contrast, the Appalachian Plateau and global models performed relatively poorly ($R^2 < 0.2$, MAPE > 40; *Table S3*). When comparing our variable importance, we observed generally low incMSE% values across all three models, suggesting that all variables were similarly important. In the Coastal Plain and Appalachian Plateaus watersheds, variables representing topographic drivers tended to be the most important, though the Coastal Plain did have several soil and vegetation parameters with positive incMSE% values (Figure 7A,C). In the Piedmont watershed, soil and vegetation properties were the two most important variables, though topographic variables also had high importance (Figure 7B). However, no one variable was the most important in all three watersheds, suggesting varying local controls over flow persistence.

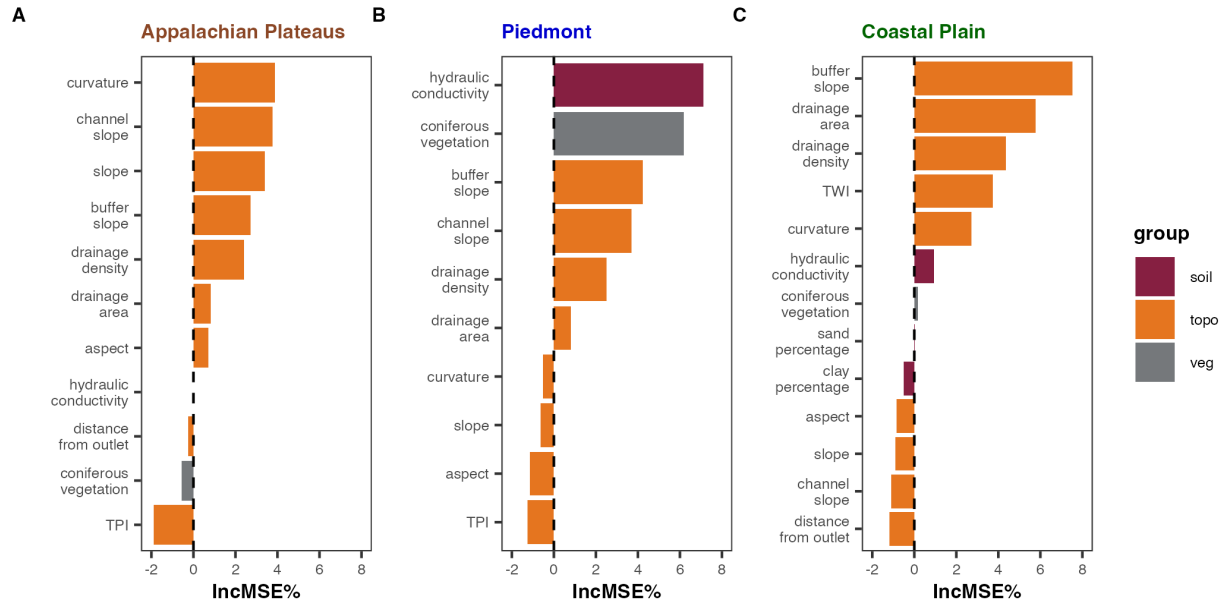


Figure 7. Results from the random forest models using data from all three watersheds. We used a random forest model to investigate the relative importance (here, percent increase in mean standard error, incMSE%) of each of our variables to predicting water persistence at any given site. Variables are ordered from most to least important, and colored by physiographic compartment (i.e., soil, topography, or vegetation; geologic variables were removed due to high correlation with other variables).

3.4 Sensor placement influenced the results of network-scale expansion and contraction

When the more extensive sensor network was deployed in the Piedmont watershed, there were key differences in the magnitude of network expansion and contraction, as well as the significant related drivers. Using only the 20 permanent sensors, the network appeared highly stable in the 2023 water year, with the smallest magnitude of network contraction across the three physiographic regions. However, when ASDN length was calculated using the high-density sensor network, the stream network was much more dynamic, expanding to 5,320 m during precipitation events, and contracting to 2,740 m during drydown (Figure 8A). Conversely, the permanent sensor network only captured a maximum expansion of 3,330 m and a minimum contraction of 2,540 m. Taken together, these results show that both sensor networks captured

similar magnitudes of contraction during the drydown, but the high-density network better captured expansion in the ephemeral headwater reaches of the network.

Further, we compared the relationships between the primary topographic drivers and site-specific water persistence using the high-density network. When considering the permanent network, there were significant correlations between water persistence for both drainage density and channel slope (Figure 5), where steeper slopes and less dense networks were significantly drier. We observed this same pattern when considering the high-density network. When comparing drainage density and water persistence, there was a significant positive correlation between drainage density and water persistence in the high-density network ($\rho = 0.73$, $p < 0.01$; Figure 8B), where increasing topographic convergence was correlated with increased water persistence. Similarly, there was a significant relationship between channel slope and water persistence in the high-density network (Figure 8C), with a highly negative correlation ($\rho = -0.79$) compared to a moderately negative correlation in the permanent network ($\rho = -0.65$). However, neither the permanent nor the high-density networks had a significant correlation between valley curvature and water persistence.

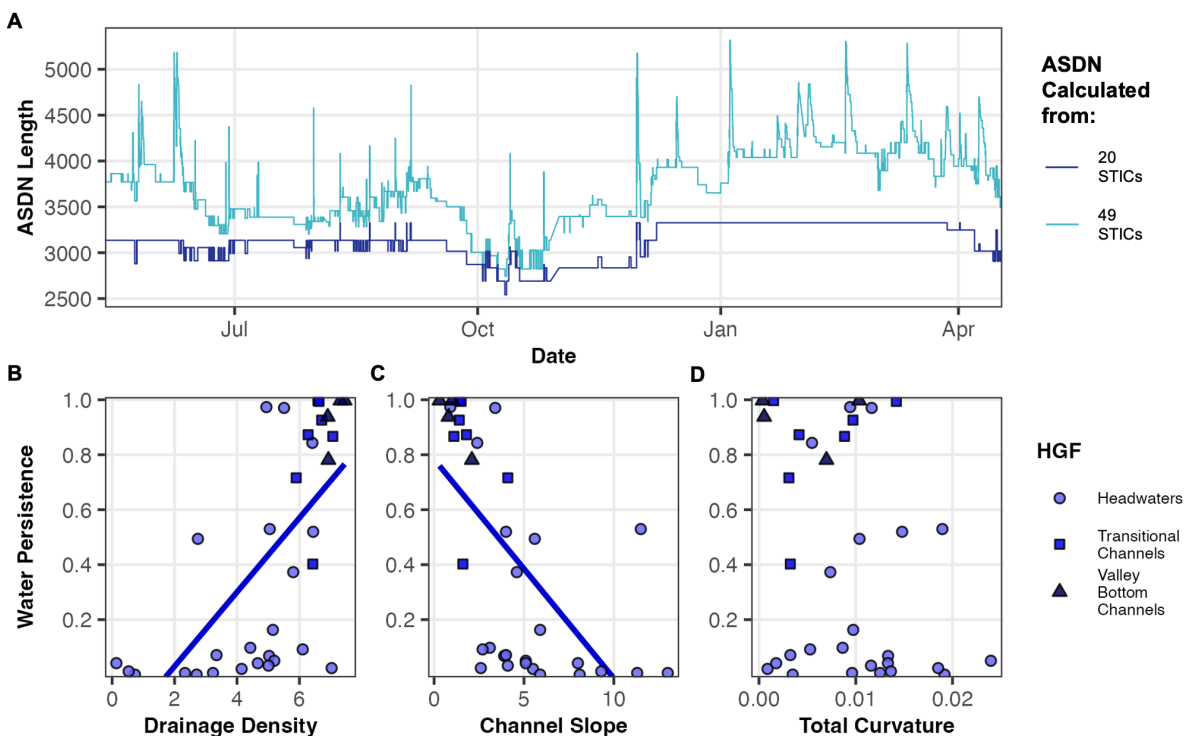


Figure 8. (A) ASDN length for the Piedmont research watershed as calculated from the

permanent ($n = 20$) sensors in dark blue and from the high-density network ($n = 49$) in light blue. **(B-D)** scatterplots of the relationships of our three primary topographic metrics when compared to the water persistence of the non-perennial STICs within the high density network ($n = 34$). Each sensor is colored by HGF.

4 Discussion

4.1 Low-relief watersheds do not conform to previously documented patterns in network expansion and contraction

Our study aimed to compare three intensively monitored watersheds in the southeastern US to existing perceptual models of topographic controls on network expansion and contraction. We found that when comparing our three research watersheds to the relationships established by Prancevic & Kirchner (2019), both of our lower-relief Piedmont and Coastal Plain watersheds aligned more with the “outlier” watersheds in their study than the rest of study watersheds (Figure 3A), primarily as a function of valley curvature and transmissivity decreasing as drainage area increases. Additionally, we found that our Piedmont watershed was highly similar to Coweeta 40 from the original study, with high transmissivity scaling exponents (γ , Coweeta = 8.21, Piedmont = 9.31), negative curvature coefficients (δ , Coweeta = -2.32, Piedmont = -2.84), and resulting negative expansion exponents (β , Coweeta = -0.14, Piedmont = -0.12, *Table S2*). This is likely a function of both the geologic settings and general proximity of these two watersheds; while Coweeta is located in the Blue Ridge physiographic province, both this region and the Piedmont are lithologically highly similar (Miller et al., 2000) as both are underlain by highly weathered metamorphic rock and separated by a fault. Further, we expect that increased subsurface complexity is likely what drove the large disparity between topographically predicted and observed β (Figure 3B).

Both the Piedmont and Coastal Plain networks were predicted to be highly dynamic, as low-relief regions often have channel-forming features that generate networks with high coefficients of variation (Prancevic et al., 2025). The Coastal Plain watershed had a higher predicted β than any of the original 17 watersheds ($\beta = 0.49$; Figure 3b). However, the observed β for both the Piedmont and Coastal Plain watersheds were among the lowest in the original study, indicating relatively stable networks. In contrast, our highest-relief watershed, the

Appalachian Plateaus, had highly similar predicted vs observed β . This indicates that the Appalachian Plateaus watershed conformed more closely to topographically derived metrics, which is further supported by the relief in this watershed being more comparable to several of the original 17 watersheds in Prancevic & Kirchner (2019).

We found that no topographic characteristic (e.g., convergence, slope, curvature) was a significant driver of water persistence in all three of our watersheds. When comparing topographic metrics to water persistence, relationships varied among watersheds, and often did not align with previously established observations. For example, while channel slope was significant for both the Piedmont and Appalachian Plateaus watersheds, it was positively correlated with water persistence in the Appalachian Plateaus, and negatively correlated in the Piedmont. Following the relationships between these topographic metrics and network expansion and contraction outlined by Prancevic & Kirchner (2019), we would expect a negative relationship, as decreasing slope would decrease subsurface flow, driving water to the surface and creating more water persistence. Therefore, the Piedmont watershed aligned with this conceptualization, which has been supported by other studies (e.g., Montgomery & Dietrich, 1995; Rinderer et al., 2014). The Appalachian Plateaus, however, demonstrated the opposite pattern, in which steeper slopes were correlated with wetter locations (see section 4.2). While this is not the first study to find that topography does not significantly explain network variability (e.g., Warix et al., 2021; Whiting & Godsey, 2016), our results suggest that low-relief watersheds do not align with these expected patterns because the complexity and interactions of other controls, such as soil structure, underlying geology, and vegetative water demand (Figure 7), are important drivers of network variability.

We observed similar dynamics for TWI, which was one of the only significant metrics for all three watersheds. We observed the expected positive correlation between water persistence and TWI for both the Piedmont and the Coastal Plain, where higher TWIs were correlated with wetter portions of the network. However, the Appalachian Plateaus watershed demonstrated the opposite pattern, where portions of the network with higher TWIs were drier than other portions of the network. Given that TWI integrates both drainage area and slope (Beven & Kirkby, 1979), the Appalachian Plateaus watershed contradicts the assumption that larger areas paired with lower slopes yield wetter conditions. We anticipate that these unexpected

patterns in topographic variables are more an expression of the bottom-up drying pattern we observed (*Figure S5*). While the standard conceptualization is that networks expand and contract from the top-down (Biswal & Marani, 2010), our Appalachian Plateaus watershed disconnected at the outlet before contracting up-network, which has only been documented in a handful of other studies (e.g., Costigan et al., 2015; Senatore et al., 2021; Zipper et al., 2025). We expect these patterns are primarily caused by the geologic setting; the Appalachian Plateaus watershed is karst, and the majority of cave-springs are located in the steeper headwaters of this network. Taken together, the lack of consistent significant topographic controls in our results points to the importance of considering all components of physiography in low-relief networks; in the absence of significant topographic variation, the heterogeneity of otherwise subordinate controls become more significant predictors of hydrologic dynamics.

4.2 Watershed-scale patterns in connectivity are driven by hierarchical interactions between topographic, geologic, and biotic variables

Hierarchical drivers interact predictably across subordinate scales to drive emergent patterns of streamflow generation and network connectivity (McDonnell et al., 2007). At large scales, there is general agreement that observable network-scale patterns in connectivity reflect and integrate hydroclimatic, geologic, and biologic conditions across both spatial and temporal scales (e.g., Godsey & Kirchner, 2014; Hynes, 1975; Newcomb & Godsey, 2023; Ward et al., 2018). Further, it has been well documented that variability in these conditions across space translates to watershed-scale variability in network connectivity (e.g., Jensen et al., 2017; Lovill et al., 2018). However, we do not yet have a clear and predictive understanding of the drivers of this network variability – and the hierarchical interactions between them – across all landscapes. For example, Hewlett & Hibbert (1967) observed that in a high-relief watershed in the Appalachian mountains, streamflow generation was controlled primarily by depth to an impervious layer, followed hierarchically by topography, climate, and land use. Other studies have documented meteorology and land use or land cover as key first-order controls on network

connectivity across scales (e.g., Costigan et al., 2016; Hammond et al., 2021; Zipper et al., 2021).

In this study we had nearly consistent meteorology and land use across our study watersheds, and yet we still observed significant differences in the network connectivity (i.e., Figure 4; similar to the findings in Lovill et al., 2018). Therefore, these observed patterns must be due to other controls, which we expect may be explained by differences in physiographic variables across these regions. Our data further support the importance of these watershed factors while also highlighting the interactions between them; there are significant relationships between water persistence and soil and vegetation characteristics in every watershed (e.g., Figure 6) along with topographic variables (e.g., Table 2). Further, we observed that across all three watersheds, variables from all physiographic compartments were similarly significant in our random forest models, suggesting that topographic, geologic, and vegetative variables were all important to predicting water persistence (Figure 7).

While topography plays a large role in how water moves through watersheds, our data highlight the importance of considering different aspects of topography across watersheds. For example, in the low relief of the Coastal Plain, our results paired with other studies suggest that where there are minimal slope changes that would normally drive flow to the surface, topographic convergence will instead drive flow generation (e.g., Montgomery & Dietrich, 1995). Additionally, the significant positive relationship between curvature and water persistence in the Coastal Plain likely reflects erosive and compressive processes that reduce downvalley flows and increase water persistence (Prancevic & Kirchner, 2019). Yet, many studies observed this pattern in curvature and transmissivity occurring as a result of bedrock fracturing and weathering processes (e.g., Miller & Dunne, 1996; Moon et al., 2017). However, in our Coastal Plain watershed where depths to bedrock are tens of meters deep, we anticipate that this pattern instead reflects the importance of stream incision and channel erosion, which affects flow generation and persistence in low-relief networks (e.g., Peterson et al., 2024). Further, we anticipate that the significant relationships between slope and water persistence in the Piedmont reflects a decrease in slope that slows subsurface valley flow, resulting in subsurface water being

forced to the surface (Prancevic et al., 2025). Together, our research watersheds represent the variability in how topographic variables can influence network expansion and contraction.

Further, our results demonstrate the role geology and resulting soil characteristics play in network connectivity. In the Appalachian Plateaus, the headwaters of the watershed were generally wetter than the valley bottom (*Figure S5*). This is aligned with our observations of finer-grained soils in the headwaters, and the relationship between saturated hydraulic conductivity and grain size (e.g., Wang et al., 2017) may help explain those patterns. Further, the headwaters of this watershed are located in the outcropping of the Bangor limestone unit, which contains a high density of caves and karst formations (Ponta, 2018). Taken together, we interpret the spatial pattern of water persistence as streamflow generation occurring from deep groundwater sources from karst formations, which persists through the steep headwaters with little soil or sediment accumulation. However, once this flow reaches the higher conductivity soils and sediments of the valley bottom, it enters subsurface storage zones, resulting in stream disconnection. Other studies have documented these disconnectivities occurring within networks as a result of heterogeneity in subsurface structure (e.g., Jensen et al., 2017; Whiting & Godsey, 2016), further reinforcing the role both geology and soil structure play within networks. These results are further supported by our observations in the Piedmont watershed, where the significantly drier headwaters also had significantly shallower depths to bedrock and higher saturated hydraulic conductivities with coarser soil textures. These soil conditions can increase transmissivity, which can contribute to lower water persistence as water is moved downvalley more efficiently (Godsey & Kirchner, 2014). Together, these two watersheds highlight the role geologic setting plays in driving network connectivity and disconnectivities.

In addition to the physical context of watersheds, our findings indicate that vegetative communities both spatially and temporally can regulate network-scale patterns in connectivity. Since all three research watersheds were forested, we interpret the timing of network contraction in the late summer and early fall as a function of vegetative water demand and transpiration during the peak growing season (*Figure 4*). The timing of network reconnection and expansion in the late fall and early winter coincides with leaf-off and vegetative dormancy, which reduces vegetative water demand (*Figure 4*). As such, the temporal patterns in network expansion and contraction are intricately linked with the timing of plant productivity and water use.

Additionally, we observed notable spatial patterns in vegetative community structure. For example, the Piedmont watershed vegetative community structure mirrored patterns in water persistence, where there was more coniferous vegetation in the drier headwaters. The coniferous vegetation could result in both more consistent vegetative water demand throughout the year (Swank et al., 1989; Young-Robertson et al., 2016) and increases in interception that decreases infiltration and soil water recharge (Rutter et al., 1975). Taken together, the network connectivity in the Piedmont watershed is likely a function of vegetative water demand; the headwaters are increasingly drier as plant-water interactions reduce subsurface water storage. This aligns with other studies that have found that vegetative patterns influence network connectivity (e.g., Lee et al., 2020; Newcomb & Godsey, 2023). Altogether, the topographic, geologic, and vegetative context of these watersheds better explains the observed patterns in network expansion and contraction than topography alone.

4.3 Within-watershed patterns in connectivity are tied to the scales of observation

Despite our standardized site design, we found that placement of sensors affected our network scale results. Generally, emergent watershed properties are based on the scales of observation, and so the patterns observed at one scale integrate all processes occurring at subordinate scales (McDonnell et al., 2007). Therefore, based on the established relationship between area accumulation and streamflow generation (e.g., Beven & Kirkby, 1979), we expected potential thresholds for stream heads to occur similarly in similarly-sized watersheds with consistent precipitation inputs (e.g., Jaeger et al., 2007; Wohl, 2018). However, the results in our Coastal Plain and Piedmont watersheds did not support this conceptualization, with the transition from non-perennial to perennial flow occurring much higher in the network in the Piedmont than the Coastal Plain (*Figures S6-7*). We expect that this is likely a function of the geologic setting of these watersheds; given the shallow and likely fractured bedrock of the Piedmont watershed, deep groundwater from fracture-flow likely contributed to streamflow in its headwaters (e.g., Boutt et al., 2010). This would generate more perennial flow higher in the network compared to the Coastal Plain, where flow persistence is likely driven by topographic

convergence, soil properties, and channel incision (e.g., Gutiérrez-Jurado et al., 2019; Montgomery & Dietrich, 1995; Peterson et al., 2024).

Our results emphasize the importance of site selection and sensor distribution on network-scale patterns. We found that better capturing the non-perennial portions of our Piedmont network strengthened the relationships between water persistence and topographic metrics. All three primary topographic metrics (i.e., drainage density, channel slope, and valley curvature, *sensu* Prancevic & Kirchner, 2019) were statistically significant predictors of water persistence when we compared the high-density network ($n = 49$) to the permanent network ($n = 20$). Additionally, the high-density network captured a larger magnitude of network expansion and contraction, though this did not significantly affect the generally low observed β .

We originally placed the permanent sensors based on the relationship between area accumulation and slope (*sensu* Zipper et al., 2025) without prior knowledge of the true dynamics of the system, which resulted in a bias towards lower, wetter portions of the network. While there is a precedent for distributing sensors randomly or evenly throughout a network to better capture a range of conditions (e.g., Jaeger & Olden, 2012; Jensen et al., 2019; Warix et al., 2021), this approach was less effective in our Piedmont watershed due to the relatively small area accumulation thresholds. However, if our sensor design had considered the potential for fracture flow to occur higher in the network, we could have distributed the sensors across a more representative gradient of wetness conditions. Therefore, our study highlights the importance of considering more than just topographic conditions when designing and deploying sensor networks.

5 Conclusions

We used a high-resolution sensor network to measure network connectivity in three watersheds spanning a physiographic gradient in the Southeastern US. We used both empirical and geospatial data to interrogate the drivers of network expansion and contraction through the lens of physiography (i.e., topography, geology, and biotic communities). We compared these results at both the watershed and site scales to identify key patterns in network connectivity. Our study found that the low-relief systems in the Southeastern US did not align with previous observations linking topography and network expansion and contraction patterns. When

comparing three primary topographic drivers (drainage density as a proxy for flow convergence, slope, and valley curvature), we found that no one driver explained the variability observed in all three watersheds; furthermore, no watershed had a significant relationship with all three topographic drivers. Previously derived relationships between topography and network connectivity overestimated the magnitude of expansion and contraction in our two lower-relief watersheds. However, by integrating physiographic drivers (e.g., soil properties, geology, and plant communities), we could better explain the network patterns observed. Additionally, we found that the placement and number of sensors influenced the significance of topographic drivers. Altogether, our study demonstrates that physiography is a useful template that can serve as a starting point for developing predictive relationships between watershed characteristics and hydrologic processes.

Acknowledgments

The authors received support from the AIMS Project (funded by the National Science Foundation, Award Number 2019603), the University of Alabama Graduate School, and the Alabama Water Institute. The authors would like to thank the US Forest Service, the Weyerhaeuser Company, and private landowner John Gully for their management and support of the research watersheds. The authors would also like to thank Dr. Jami Nettles, Dr. Ashleigh Kirker, Helen Czech, Patience Knight, Lidia Molina Serpas, Justus King, Caroline Anscombe, Jacob Ackerman, Kevin Shaw, Jasmine Morejon, Stella Wilson, Vanessa Marshall, and many other friends and colleagues for their help with instrument maintenance, site management, and fieldwork. The authors declare no conflicts of interest relevant to this study.

Open Research

All data used in this study are available through CUAHSI HydroShare in the public AIMS Data group (<https://www.hydroshare.org/group/247>), and are cited in appropriate locations within the text and linked in the references below. Associated analyses and scripts can be accessed at: https://github.com/dmpeterson2/STIC_physiographic_analyses#

References

- Alabama Historical Commission. (2002). The History of Agriculture in Alabama: A Historic Context. Retrieved from <https://ahc.alabama.gov/architecturalprogramsPDFs/History%20of%20Agriculture%20in%20Alabama.pdf>
- Beven, K. J., & Kirkby, M. J. (1979). A physically based, variable contributing area model of basin hydrology / Un modèle à base physique de zone d'appel variable de l'hydrologie du bassin versant. *Hydrological Sciences Bulletin*, 24(1), 43–69. <https://doi.org/10.1080/02626667909491834>
- Biswal, B., & Marani, M. (2010). Geomorphological origin of recession curves. *Geophysical Research Letters*, 37(24). <https://doi.org/10.1029/2010GL045415>
- Botter, G., & Durighetto, N. (2020). The Stream Length Duration Curve: A Tool for Characterizing the Time Variability of the Flowing Stream Length. *Water Resources Research*, 56. <https://doi.org/10.1029/2020WR027282>
- Botter, G., McNamara, J., & Durighetto, N. (2024). Extending Active Network Length Versus Catchment Discharge Relations to Temporarily Dry Outlets. *Water Resources Research*, 60(1), e2023WR035617. <https://doi.org/10.1029/2023WR035617>
- Boutt, D. F., Diggins, P., & Mabee, S. (2010). A field study (Massachusetts, USA) of the factors controlling the depth of groundwater flow systems in crystalline fractured-rock terrain. *Hydrogeology Journal*, 18(8), 1839–1854. <https://doi.org/10.1007/s10040-010-0640-y>
- Brinkerhoff, C. B., Gleason, C. J., Kotchen, M. J., Kysar, D. A., & Raymond, P. A. (2024). Ephemeral stream water contributions to United States drainage networks. *Science*, 384(6703), 1476–1482. <https://doi.org/10.1126/science.adg9430>
- Burke, E., Wilhelm, J., Zipper, S., & Brown, C. (2024). AIMS SOP STIC Calibration. CUAHSI HydroShare. Retrieved from <https://hydroshare.org/resource/9f2027c779d64149be32bdb9eede54f2/>
- Burt, T. P., & McDonnell, J. J. (2015). Whither field hydrology? The need for discovery science and outrageous hydrological hypotheses. *Water Resources Research*, 51(8), 5919–5928. <https://doi.org/10.1002/2014WR016839>

- Busch, M. H., Costigan, K. H., Fritz, K. M., Datry, T., Krabbenhoft, C. A., Hammond, J. C., et al. (2020). What's in a Name? Patterns, Trends, and Suggestions for Defining Non-Perennial Rivers and Streams. *Water*, *12*(7), 1980. <https://doi.org/10.3390/w12071980>
- Chapin, T. P., Todd, A. S., & Zeigler, M. P. (2014). Robust, low-cost data loggers for stream temperature, flow intermittency, and relative conductivity monitoring. *Water Resources Research*, *50*(8), 6542–6548. <https://doi.org/10.1002/2013WR015158>
- Chescheir, G. M., Nettles, J. E., Youssef, M., Birgand, F., Amatya, D. M., Miller, D. A., et al. (2018). Optimization of Southeastern Forest Biomass Crop Production: A Watershed Scale Evaluation of the Sustainability and Productivity of Dedicated Energy Crop and Woody Biomass Operations (No. DOE-NCSU--04395). North Carolina State Univ., Raleigh, NC (United States). <https://doi.org/10.2172/1437923>
- Cook, T. A. (1982). Stratigraphy and structure of the central Talladega slate belt, Alabama Appalachians. In D. N. Bearce, W. W. Black, S. A. Kish, & J. F. Tull (Eds.), *Tectonic Studies in the Talladega and Carolina Slate Belts, Southern Appalachian Orogen* (p. 0). Geological Society of America. <https://doi.org/10.1130/SPE191-p47>
- Costigan, K. H., Daniels, M. D., & Dodds, W. K. (2015). Fundamental spatial and temporal disconnections in the hydrology of an intermittent prairie headwater network. *Journal of Hydrology*, *522*, 305–316. <https://doi.org/10.1016/j.jhydrol.2014.12.031>
- Costigan, K. H., Jaeger, K. L., Goss, C. W., Fritz, K. M., & Goebel, P. C. (2016a). Understanding controls on flow permanence in intermittent rivers to aid ecological research: integrating meteorology, geology and land cover. *Ecohydrology*, *9*(7), 1141–1153. <https://doi.org/10.1002/eco.1712>
- Datry, T., Boulton, A. J., Bonada, N., Fritz, K., Leigh, C., Sauquet, E., et al. (2018). Flow intermittence and ecosystem services in rivers of the Anthropocene. *The Journal of Applied Ecology*, *55*(1), 353–364. <https://doi.org/10.1111/1365-2664.12941>
- Dobbs, N. A. (2016). Hydrology and Water Quality Dynamics in Coastal Plain and Upland Watersheds with Loblolly Pine (*Pinus taeda*) and Switchgrass (*Panicum virgatum*) Intercropping in the southeastern United States. Retrieved from <http://www.lib.ncsu.edu/resolver/1840.20/33346>

- Dohman, J. M., Godsey, S. E., & Hale, R. L. (2021). Three-Dimensional Subsurface Flow Path Controls on Flow Permanence. *Water Resources Research*, 57(10), e2020WR028270. <https://doi.org/10.1029/2020WR028270>
- Feminella, J. W. (1996). Comparison of Benthic Macroinvertebrate Assemblages in Small Streams along a Gradient of Flow Permanence. *Journal of the North American Benthological Society*, 15(4), 651–669. <https://doi.org/10.2307/1467814>
- Fenneman, N. M. (1938). *Physiography of eastern United States*. McGraw-Hill Book Company, inc. Retrieved from <http://archive.org/details/physiographyofea0000nevi>
- Fickle, J. (2014). Green Gold. Retrieved June 20, 2025, from <https://www.uapress.ua.edu/9780817318130/green-gold/>
- Florinsky, I. V. (2016). Chapter 1 - Digital Terrain Modeling: A Brief Historical Overview. In I. V. Florinsky (Ed.), *Digital Terrain Analysis in Soil Science and Geology* (Second Edition) (pp. 1–4). Academic Press. <https://doi.org/10.1016/B978-0-12-804632-6.00001-8>
- Godsey, S., Wheeler, C., & Zipper, S. (2024). AIMS SOP STIC Deployment and Maintenance | CUAHSI HydroShare. CUAHSI HydroShare. Retrieved from <https://hydroshare.org/resource/c82a87a6c63445029d35131260241386/>
- Godsey, S. E., & Kirchner, J. W. (2014). Dynamic, discontinuous stream networks: hydrologically driven variations in active drainage density, flowing channels and stream order. *Hydrological Processes*, 28(23), 5791–5803. <https://doi.org/10.1002/hyp.10310>
- Golden, H. E., Christensen, J. R., McMillan, H. K., Kelleher, C. A., Lane, C. R., Husic, A., et al. (2025). Advancing the science of headwater streamflow for global water protection. *Nature Water*, 1–11. <https://doi.org/10.1038/s44221-024-00351-1>
- Gómez-Gener, L., Siebers, A. R., Arce, M. I., Arnon, S., Bernal, S., Bolpagni, R., et al. (2021). Towards an improved understanding of biogeochemical processes across surface-groundwater interactions in intermittent rivers and ephemeral streams. *Earth-Science Reviews*, 220, 103724. <https://doi.org/10.1016/j.earscirev.2021.103724>
- Griffith, G. E., Omernik, J. M., Comstock, J. A., Lawrence, S., Martin, G., Goddard, A., et al. (2001). Ecoregions of Alabama. U.S. Environmental Protection Agency, National Health and Environmental Effects Research Laboratory, Corvallis, OR.

- Gutiérrez-Jurado, K. Y., Partington, D., Batelaan, O., Cook, P., & Shanafield, M. (2019). What Triggers Streamflow for Intermittent Rivers and Ephemeral Streams in Low-Gradient Catchments in Mediterranean Climates. *Water Resources Research*, *55*(11), 9926–9946. <https://doi.org/10.1029/2019WR025041>
- Hammond, J. C., Zimmer, M., Shanafield, M., Kaiser, K., Godsey, S. E., Mims, M. C., et al. (2021). Spatial patterns and drivers of non-perennial flow regimes in the contiguous U.S. *Geophysical Research Letters*, *n/a*(*n/a*), 2020GL090794. <https://doi.org/10.1029/2020GL090794>
- Harvey, J., & Gooseff, M. (2015). River corridor science: Hydrologic exchange and ecological consequences from bedforms to basins. *Water Resources Research*, *51*(9), 6893–6922. <https://doi.org/10.1002/2015WR017617>
- Hewlett, J., & Hibbert, A. (1967). Factors Affecting the Response of Small Watersheds to Precipitation in Humid Areas. In *Proceedings of the International Symposium on Forest Hydrology*. Pergamon, Pennsylvania State University, NY.
- Hynes, H. B. N. (1975). The stream and its valley. *SIL Proceedings, 1922-2010*, *19*(1), 1–15. <https://doi.org/10.1080/03680770.1974.11896033>
- Ilich, A., Lecours, V., Misiuk, B., & Murawski, S. (2025). MultiscaleDTM: Multi-Scale Geomorphometric Terrain Attributes (Version 1.0). Retrieved from <https://cran.r-project.org/web/packages/MultiscaleDTM/index.html>
- Jaeger, K. L., & Olden, J. D. (2012). Electrical Resistance Sensor Arrays as a Means to Quantify Longitudinal Connectivity of Rivers. *River Research and Applications*, *28*(10), 1843–1852. <https://doi.org/10.1002/rra.1554>
- Jaeger, Kristin L., Montgomery, D. R., & Bolton, S. M. (2007). Channel and Perennial Flow Initiation in Headwater Streams: Management Implications of Variability in Source-Area Size. *Environmental Management*, *40*(5), 775–786. <https://doi.org/10.1007/s00267-005-0311-2>
- Jensen, C. K., McGuire, K. J., & Prince, P. S. (2017). Headwater stream length dynamics across four physiographic provinces of the Appalachian Highlands. *Hydrological Processes*, *31*(19), 3350–3363. <https://doi.org/10.1002/hyp.11259>
- Jensen, C. K., McGuire, K. J., McLaughlin, D. L., & Scott, D. T. (2019). Quantifying spatiotemporal variation in headwater stream length using flow intermittency sensors.

Environmental Monitoring and Assessment, 191(4), 226. <https://doi.org/10.1007/s10661-019-7373-8>

- Jones, C. N., Nelson, N. G., & Smith, L. L. (2019). Featured Collection Introduction: The Emerging Science of Aquatic System Connectivity I. *JAWRA Journal of the American Water Resources Association*, 55(2), 287–293. <https://doi.org/10.1111/1752-1688.12739>
- Kidd, R. E., & Lambeth, D. S. (1995). HYDROGEOLOGY AND GROUND-WATER QUALITY IN THE BLACK BELT AREA OF WEST-CENTRAL ALABAMA, AND ESTIMATED WATER USE FOR AQUACULTURE, 1990 (Water-Resources Investigations Report No. 94–4074). Tuscaloosa, Alabama: U.S. Geological Survey. Retrieved from https://web.archive.org/web/20190501065314id_/https://pubs.usgs.gov/wri/1994/4074/report.pdf
- Kindred, T. (2022). *Spatial Structure, Temporal Patterns, and Drivers of Stream Drying In the Gibson Jack Watershed, Bannock County, Idaho*. Idaho State University, Pocatello, ID.
- Kopaska-Merkel, D. C., Dean, L. S., & Moore, J. D. (2000). HYDROGEOLOGY AND VULNERABILITY TO CONTAMINATION OF MAJOR AQUIFERS IN ALABAMA: AREA 5.
- Lee, S., McCarty, G. W., Moglen, G. E., Lang, M. W., Nathan Jones, C., Palmer, M., et al. (2020). Seasonal drivers of geographically isolated wetland hydrology in a low-gradient, Coastal Plain landscape. *Journal of Hydrology*, 583, 124608. <https://doi.org/10.1016/j.jhydrol.2020.124608>
- Liaw, A., & Wiener, M. (2024). randomForest: Breiman and Cutlers Random Forests for Classification and Regression (Version 4.7-1.2). Retrieved from <https://cran.r-project.org/web/packages/randomForest/index.html>
- Lindsay, J. B. (2016). Whitebox GAT: A case study in geomorphometric analysis. *Computers & Geosciences*, 95, 75–84. <https://doi.org/10.1016/j.cageo.2016.07.003>
- Lovill, S. M., Hahm, W. J., & Dietrich, W. e. (2018). Drainage from the Critical Zone: Lithologic Controls on the Persistence and Spatial Extent of Wetted Channels during the Summer Dry Season. *Water Resources Research*, 54(8), 5702–5726. <https://doi.org/10.1029/2017WR021903>

- McDonnell, J. J., Sivapalan, M., Vaché, K., Dunn, S., Grant, G., Haggerty, R., et al. (2007). Moving beyond heterogeneity and process complexity: A new vision for watershed hydrology. *Water Resources Research*, *43*(7). <https://doi.org/10.1029/2006WR005467>
- McMillan, H., Araki, R., Gnann, S., Woods, R., & Wagener, T. (2023). How do hydrologists perceive watersheds? A survey and analysis of perceptual model figures for experimental watersheds. *Hydrological Processes*, *37*(3), e14845. <https://doi.org/10.1002/hyp.14845>
- Messenger, M. L., Lehner, B., Cockburn, C., Lamouroux, N., Pella, H., Snelder, T., et al. (2021). Global prevalence of non-perennial rivers and streams. *Nature*, *594*(7863), 391–397. <https://doi.org/10.1038/s41586-021-03565-5>
- Miller, C. F., Hatcher, R. D., Ayers, J. C., Coath, C. D., & Harrison, T. M. (2000). Age and zircon inheritance of eastern Blue Ridge plutons, southwestern North Carolina and northeastern Georgia, with implications for magma history and evolution of the southern Appalachian orogen. *American Journal of Science*, *300*, 142–172.
- Miller, D. J., & Dunne, T. (1996). Topographic perturbations of regional stresses and consequent bedrock fracturing. *Journal of Geophysical Research: Solid Earth*, *101*(B11), 25523–25536. <https://doi.org/10.1029/96JB02531>
- Montgomery, D. R., & Dietrich, W. E. (1989). Source areas, drainage density, and channel initiation. *Water Resources Research*, *25*(8), 1907–1918. <https://doi.org/10.1029/WR025i008p01907>
- Montgomery, D. R., & Dietrich, W. E. (1995). Hydrologic Processes in a Low-Gradient Source Area. *Water Resources Research*, *31*(1), 1–10. <https://doi.org/10.1029/94WR02270>
- Moon, S., Perron, J. T., Martel, S. J., Holbrook, W. S., & St. Clair, J. (2017). A model of three-dimensional topographic stresses with implications for bedrock fractures, surface processes, and landscape evolution. *Journal of Geophysical Research: Earth Surface*, *122*(4), 823–846. <https://doi.org/10.1002/2016JF004155>
- Newcomb, S. K., & Godsey, S. E. (2023). Nonlinear Riparian Interactions Drive Changes in Headwater Streamflow. *Water Resources Research*, *59*(10), e2023WR034870. <https://doi.org/10.1029/2023WR034870>
- NOAA National Centers for Environmental information. (2023). Climate at a Glance: County Time Series [Data set]. Retrieved from <https://www.ncei.noaa.gov/access/monitoring/climate-at-a-glance/county/time-series>

- Peterson, D., N. Jones (2025). Paint Rock Environmental Data (AIMS_SE_PRF_ENVI), HydroShare, <http://www.hydroshare.org/resource/656211b1a1484433a3bc524fb968b4bd>
- Peterson, D., N. Jones (2025). Shambley Creek Environmental Data (AIMS_SE_WHR_ENVI), HydroShare, <http://www.hydroshare.org/resource/126d2c7b1c8d4889a8ccc454d387b0d8>
- Peterson, D., N. Jones (2025). Talladega Environmental Data (AIMS_SE_TAL_ENVI), HydroShare, <http://www.hydroshare.org/resource/81c003a7b8474d63a31641a4f375fd18>
- Peterson, D., N. Jones (2025). Paint Rock Meteorological Data (AIMS_SE_PRF_approach1_METS), HydroShare, <http://www.hydroshare.org/resource/4089918c0a494bfeb19be0421a33d297>
- Peterson, D., N. Jones (2025). Shambley Creek Meteorological Data (AIMS_SE_WHR_approach1_METS), HydroShare, <http://www.hydroshare.org/resource/33823d8603ce439fbba48fbcbbba22da4>
- Peterson, D., N. Jones (2025). Talladega Meteorological Data (AIMS_SE_TAL_approach1_METS), HydroShare, <http://www.hydroshare.org/resource/281cd7627629481dbdc7d4ccf6fcfbcc>
- Peterson, D., N. Jones (2025). Paint Rock Pressure Transducer Data (AIMS_SE_PRF_approach1_PRES), HydroShare, <http://www.hydroshare.org/resource/a45b5e24dafc4a76a665405664afada7>
- Peterson, D., N. Jones (2025). Shambley Creek Pressure Transducer Data (AIMS_SE_WHR_approach1_PRES), HydroShare, <http://www.hydroshare.org/resource/bc34c8b51c514bf4a6e0a44493bf8ca3>
- Peterson, D., N. Jones (2025). Talladega Pressure Transducer Data (AIMS_SE_TAL_approach1_PRES), HydroShare, <http://www.hydroshare.org/resource/93e2861410e647d9a710eea036832dbe>
- Peterson, D., N. Jones (2025). Paint Rock Stream Temperature, Intermittency, and Conductivity Data (AIMS_SE_PRF_approach1_STIC), HydroShare, <http://www.hydroshare.org/resource/d57338ebfb0240f58e8de37ddacf9426>
- Peterson, D., N. Jones (2025). Shambley Creek Stream Temperature, Intermittency, and Conductivity Data (AIMS_SE_WHR_approach1_STIC), HydroShare, <http://www.hydroshare.org/resource/dc623510ed1847f8abe1275904472c44>

- Peterson, D., N. Jones (2025). Talladega Stream Temperature, Intermittency, and Conductivity Data (AIMS_SE_TAL_approach1_STIC), HydroShare, <http://www.hydroshare.org/resource/ff306bec9fb24e52aa809dbb4d074731>
- Peterson, D. M., Jones, C. N., Plattner, A., Shogren, A., & Godsey, S. E. (2024). Using Hydrogeomorphic Features to Quantify Structural and Functional Hydrologic Connectivity in a Coastal Plain Headwater Stream [pre-print]. Retrieved from <https://eartharxiv.org/repository/view/7478/>
- Ponta, G. (2018). Geologic Framework of Karst Aquifer Systems in Alabama. *Sinkhole Conference 2018*. Retrieved from https://digitalcommons.usf.edu/sinkhole_2018/ProceedingswithProgram/Appalachian_Karst/6
- Prancevic, J. P., & Kirchner, J. W. (2019). Topographic Controls on the Extension and Retraction of Flowing Streams. *Geophysical Research Letters*, *46*(4), 2084–2092. <https://doi.org/10.1029/2018GL081799>
- Prancevic, J. P., Seybold, H., & Kirchner, J. W. (2025). Variability of flowing stream network length across the US. *Science*, *387*(6735), 782–786. <https://doi.org/10.1126/science.ado2860>
- Pringle, C. M. (2001). Hydrologic Connectivity and the Management of Biological Reserves: A Global Perspective. *Ecological Applications*, *11*(4), 981–998. [https://doi.org/10.1890/1051-0761\(2001\)011\[0981:HCATMO\]2.0.CO;2](https://doi.org/10.1890/1051-0761(2001)011[0981:HCATMO]2.0.CO;2)
- R Core Team. (2024). R: A Language and Environment for Statistical Computing. Vienna, Austria: R Foundation for Statistical Computing. Retrieved from <https://www.R-project.org/>
- Rinderer, M., van Meerveld, H. J., & Seibert, J. (2014). Topographic controls on shallow groundwater levels in a steep, prealpine catchment: When are the TWI assumptions valid? *Water Resources Research*, *50*(7), 6067–6080. <https://doi.org/10.1002/2013WR015009>
- Rinderer, M., Ali, G., & Larsen, L. G. (2018). Assessing structural, functional and effective hydrologic connectivity with brain neuroscience methods: State-of-the-art and research directions. *Earth-Science Reviews*, *178*, 29–47. <https://doi.org/10.1016/j.earscirev.2018.01.009>

- Roberts, M., & Klingeman, P. (1972). The relationship of drainage net fluctuation and discharge. Proc. Internat. Geographical Congress, 181–191.
- Rutter, A. J., Morton, A. J., & Robins, P. C. (1975). A Predictive Model of Rainfall Interception in Forests. II. Generalization of the Model and Comparison with Observations in Some Coniferous and Hardwood Stands. *Journal of Applied Ecology*, 12(1), 367–380.
<https://doi.org/10.2307/2401739>
- Sapp, C. D., & Emplaincourt, J. (1975). Physiographic regions of Alabama. Geological Survey of Alabama. Retrieved from https://ngmdb.usgs.gov/Prodesc/proddesc_55813.htm
- Senatore, A., Micieli, M., Liotti, A., Durighetto, N., Mendicino, G., & Botter, G. (2021). Monitoring and Modeling Drainage Network Contraction and Dry Down in Mediterranean Headwater Catchments. *Water Resources Research*, 57(6), e2020WR028741. <https://doi.org/10.1029/2020WR028741>
- Shaw, S. B. (2016). Investigating the linkage between streamflow recession rates and channel network contraction in a mesoscale catchment in New York state. *Hydrological Processes*, 30(3), 479–492. <https://doi.org/10.1002/hyp.10626>
- Soil Survey Staff, Natural Resources Conservation Service, USDA. Accessed March 2025. Web Soil Survey [Data set]. Retrieved from <https://websoilsurvey.nrcs.usda.gov/app/>
- Swenson, G. A. (1954). *Soil Survey of Jackson County, Alabama*. U.S. Department of Agriculture, Soil Conservation Service.
- Swenson, L. J., Zipper, S., Peterson, D. M., Jones, C. N., Burgin, A. J., Seybold, E., et al. (2024). Changes in Water Age During Dry-Down of a Non-Perennial Stream. *Water Resources Research*, 60(1), e2023WR034623. <https://doi.org/10.1029/2023WR034623>
- Swank, W., DeBano, L., & Nelson, D. (1989). Effects of Timber Management Practices on Soil and Water. In *The Scientific Basis for Silvicultural and Management Decisions in the National Forest System*. U.S. Department of Agriculture, Forest Service.
- Szabo, E. W., Osborne, W. E., Copeland, C. W., & Neathery, T. L. (1988). Geologic map of Alabama. Geological Survey of Alabama. Retrieved from https://ngmdb.usgs.gov/Prodesc/proddesc_55859.htm
- Trimble, S. W. (2008). *Man-Induced Soil Erosion on the Piedmont, 1700-1970* (2nd ed.). Ankeny, IA: Soil and Water Conservation Society.

- Wahl, K. D. (1966). Geology and ground-water resources of Greene County, Alabama. Geological Survey of Alabama. Retrieved from https://ngmdb.usgs.gov/Prodesc/proddesc_55588.htm
- Wang, J.-P., François, B., & Lambert, P. (2017). Equations for hydraulic conductivity estimation from particle size distribution: A dimensional analysis. *Water Resources Research*, 53(9), 8127–8134. <https://doi.org/10.1002/2017WR020888>
- Ward, A. S., Schmadel, N. M., & Wondzell, S. M. (2018). Simulation of dynamic expansion, contraction, and connectivity in a mountain stream network. *Advances in Water Resources*, 114, 64–82. <https://doi.org/10.1016/j.advwatres.2018.01.018>
- Ward, J. V. (1989). The Four-Dimensional Nature of Lotic Ecosystems. *Journal of the North American Benthological Society*, 8(1), 2–8. <https://doi.org/10.2307/1467397>
- Warix, S. R., Navarre-Sitchler, A., Manning, A. H., & Singha, K. (2023). Local Topography and Streambed Hydraulic Conductivity Influence Riparian Groundwater Age and Groundwater-Surface Water Connection. *Water Resources Research*, 59(9), e2023WR035044. <https://doi.org/10.1029/2023WR035044>
- Warix, S. R., Godsey, S. E., Lohse, K. A., & Hale, R. L. (2021). Influence of groundwater and topography on stream drying in semi-arid headwater streams. *Hydrological Processes*, 35(5), e14185. <https://doi.org/10.1002/hyp.14185>
- Whiting, J. A., & Godsey, S. E. (2016). Discontinuous headwater stream networks with stable flowheads, Salmon River basin, Idaho. *Hydrological Processes*, 30(13), 2305–2316. <https://doi.org/10.1002/hyp.10790>
- Wilson, J. (2018). Calculating Land Surface Parameters. In *Environmental Applications of Digital Terrain Modeling* (pp. 53–149). John Wiley & Sons, Ltd. <https://doi.org/10.1002/9781118938188.ch3>
- Wohl, E. (2018). The challenges of channel heads. *Earth-Science Reviews*, 185, 649–664. <https://doi.org/10.1016/j.earscirev.2018.07.008>
- Wu, Q., & Brown, A. (2022). whitebox: “WhiteboxTools” R Frontend. R package version 2.2.0. Retrieved from <https://CRAN.R-project.org/package=whitebox>
- Young-Robertson, J. M., Bolton, W. R., Bhatt, U. S., Cristóbal, J., & Thoman, R. (2016). Deciduous trees are a large and overlooked sink for snowmelt water in the boreal forest. *Scientific Reports*, 6(1), 29504. <https://doi.org/10.1038/srep29504>

- Zanetti, F., Botter, G., & Camporese, M. (2024). Stream Network Dynamics of Non-Perennial Rivers: Insights From Integrated Surface-Subsurface Hydrological Modeling of Two Virtual Catchments. *Water Resources Research*, *60*(2), e2023WR035631.
<https://doi.org/10.1029/2023WR035631>
- Zarek, K., Jones, C. N., Peterson, D. M., Plont, S., Shogren, A. J., Tatariw, C., et al. (2025). Investigating Spatial and Temporal Nitrogen Dynamics in a Forested Headwater Stream Over the Course of an Annual Drying Event. *Journal of Geophysical Research: Biogeosciences*, *130*(4), e2024JG008522. <https://doi.org/10.1029/2024JG008522>
- Zimmer, M. A., & McGlynn, B. L. (2017). Bidirectional stream–groundwater flow in response to ephemeral and intermittent streamflow and groundwater seasonality. *Hydrological Processes*, *31*(22), 3871–3880. <https://doi.org/10.1002/hyp.11301>
- Zimmer, M. A., & McGlynn, B. L. (2018). Lateral, Vertical, and Longitudinal Source Area Connectivity Drive Runoff and Carbon Export Across Watershed Scales. *Water Resources Research*, *54*(3), 1576–1598. <https://doi.org/10.1002/2017WR021718>
- Zimmer, M. A., Burgin, A. J., Kaiser, K., & Hosen, J. (2022). The unknown biogeochemical impacts of drying rivers and streams. *Nature Communications*, *13*(1), 7213.
<https://doi.org/10.1038/s41467-022-34903-4>
- Zipper, S., Wheeler, C. T., Peterson, D. M., Cook, S. C., Godsey, S. E., & Aho, K. (2025). STICr: An open-source package and workflow for stream temperature, intermittency, and conductivity (STIC) data. *Environmental Modelling & Software*, *190*, 106484.
<https://doi.org/10.1016/j.envsoft.2025.106484>
- Zipper, S. C., Hammond, J. C., Shanafield, M., Zimmer, M., Datry, T., Jones, C. N., et al. (2021). Pervasive changes in stream intermittency across the United States. *Environmental Research Letters*, *16*(8), 084033. <https://doi.org/10.1088/1748-9326/ac14ec>

Water Resources Research

Supporting Information for

**Using Physiography as a Lens to Understand Stream Network Expansion and Contraction
Across Spatiotemporal Scales**

Delaney M. Peterson¹, C. Nathan Jones¹, Kaci Zarek^{1,2}, Michelle Wolford¹, Chelsea R. Smith¹, Charles T. Bond³, Stephen Plont¹, Maggi Kraft⁴, Shannon Speir⁵, Sam Zipper^{6,7}, Sarah E. Godsey⁴, Jonathan P. Benstead¹, Ariel J. Shogren¹, Kevin A. Kuehn³, and Carla L. Atkinson¹

¹Department of Biological Sciences, University of Alabama, Tuscaloosa, AL, USA.

²Department of Ecology and Evolutionary Biology, Cornell University, Ithaca, NY, USA.

³School of Biological, Environmental, and Earth Sciences, University of Southern Mississippi, Hattiesburg, MS, USA.

⁴Department of Geosciences, Idaho State University, Pocatello, ID, USA.

⁵Department of Crop, Soil, and Environmental Sciences, University of Arkansas, Fayetteville, AR, USA.

⁶Kansas Geological Survey, Lawrence, KS, USA.

⁷Department of Geology, University of Kansas, Lawrence, KS, USA.

Contents of this file

Text S1

Figures S1 to S7

Tables S1 to S3

Introduction

This document contains more detailed site information (Text S1), study design and sensor placement (Figures S1-4), description of all physiographic metrics (Table 1), and additional analyses and statistical results (Table 2-3), and additional figures that provide more context to results (Figures S5-7).

Text S1 – Detailed Site Descriptions.

We instrumented three research watersheds across a physiographic gradient in Alabama, USA to evaluate network expansion and contraction across comparably-sized non-perennial streams. In addition to the details provided in Section 2.1 and Table 1, we have included more detailed watershed characteristics below.

Appalachian Plateau Research Watershed

The research watershed in the Appalachian Plateau province drains 2.97km² of Fanning Hollow and Miller Mountain to form the steep headwaters of Burks Creek, within the larger Paint Rock River and Tennessee River basins. Physiographically, this research watershed is in the Jackson Mountains district, defined by flat sandstone-capped ridges that are highly dissected by dendritic stream networks that form V-shaped ravines and rock-walled gorges as they grade into wider valley bottoms (Swenson, 1945; Sapp & Emplincourt, 1975).

Geologically, this watershed cuts through and exposes several distinct sedimentary lithologic units. In this region, the plateaus are primarily from the Pottsville and Pennington Formations, which are underlain by the Bangor limestone, Monteagle limestone, and Tuscumbia limestone units, respectively (Szabo et al., 1988; Ponta, 2018). The Pottsville and Pennington formations are primarily sandstones and shales interbedded with limestone, dolomite, and mudstones, whereas the three underlying units are primarily limestone and dolomite with some chert concretions in the Tuscumbia unit (Szabo et al., 1988). Further, the Bangor, Monteagle, and Tuscumbia limestone units are all karst, with the majority of caves in the state occurring in the Bangor limestone unit (Ponta, 2018). The Pottsville formation, Bangor limestone, and Tuscumbia limestone are the primary water-bearing units for the region, with the Pottsville formation being the largest water source in the region and the Bangor limestone being an unconfined karst aquifer that discharges through many springs (Ponta, 2018). This watershed primarily has SSURGO soil map units of Limestone rockland rough and Muskingum Rough stony land. These map units consist of highly organic soils and limestone residuum in the headwaters, and more developed, argillic soils in the valley bottom (Soil Survey Staff, 2025). The dominant soil series are the Barfield, Gorgas, and Egam series.

This watershed is located in the Plateau Escarpment level IV ecoregion, and therefore the forest structure is primarily deciduous, with mixed oak species (chestnut oak, white and red oaks) in the upper slopes, mesic forest (beech, yellow-poplar, sugar maple, basswood, ash, buckeye) in the middle and lower slopes, and some hemlock and river birch in the riparian zones and floodplain terraces near the outlet (Griffith et al., 2001).

Piedmont Research Watershed

The research watershed in the Piedmont province drains 0.92km² of Rattlesnake Mountain to form the headwaters of Pendergrass Creek, within the larger Coosa River and Mobile-Tombigbee River basins. Physiographically, this watershed is in the Northern Piedmont Upland district, defined as a well-dissected mature upland in the transition between the nearby Ridge and Valley and Coastal Plain regions (Kopaska-Merkel et al., 2000).

Geologically, this watershed is underlain by fractured metamorphic lithologic units. The watershed is located in the Talladega belt near the Talladega fault, and lies within the exposed Lay Dam formation, which is made up of interbedded phyllite, metasiltstone, and quartzite members (Szabo et al, 1988; Cook, 1982; Kopaska-Merkel et al., 2000). Productivity of the groundwater system in the Piedmont is driven by fractures rather than geologic material (Kopaska-Merkel et al., 2000), and the proximity of this location to the Talladega fault has likely resulted in a productive groundwater system where the fractures intersect with the soil and ground surface. This watershed has highly weathered soils, with the primary soil series being the Cheaha, Tatum, and Fruithurst, as well as some more organic, fine-grained soils near the watershed outlet (Soil Survey Staff, 2025; Zarek et al., 2025).

The watershed is located within the Talladega Upland level IV ecoregion, and therefore has a mixed deciduous-coniferous forest structure. The region has an oak-hickory-pine natural vegetation type and historically contained unique montane longleaf pine communities (Griffith et al., 2001). The watershed now contains primarily pine and oak species (loblolly, longleaf, mixed red and white oaks; Feminella, 1996; Zarek et al., 2025). While the larger region has a long-term land-use history of intensive cultivation (Trimble, 2008, Griffith et al., 2001), the region transitioned to silviculture around the turn of the 20th century. Additionally, the US Forest Service maintains a regular burn schedule within the National Forest to preserve the longleaf pine and endangered red cockaded woodpecker habitat. As a result, this watershed experienced low-intensity prescribed burns in the early spring of both 2022 and 2024.

Coastal Plain Research Watershed

The research watershed in the Coastal Plain province drains 0.70km² of the headwaters of Shambley Creek, within the larger Sipsey River and Mobile-Tombigbee River basins. Physiographically, this watershed is in the Fall Line Hills district, defined by low-gradient sandy uplands that are dissected by severely entrenched streams (Kidd & Lambeth, 1995; Fenneman, 1938).

Geologically, this watershed is underlain by sedimentary lithologic units. The watershed is located in the exposed Eutaw Formation, which consists of interbedded sand and clay layers (Szabo et al., 1988). This formation includes the Tombigbee Sand Member, and the shallow depth to this aquifer results in this unit being an integral water-bearing unit for the region (Wahl, 1966). The primary soils present in this watershed are the Magnolia, Shubuta, Falaya, and Ochlockonee series (Soil Survey Staff, 2025).

Greene County, as well as the larger Coastal Plain of the Southeastern US, has a long-term land-use legacy of intensive agriculture that has resulted in soil degradation and erosion (Trimble, 2008; AL Historical Commission, 2002). The region was heavily used for cotton farming throughout the 19th century before conversion to pine plantations and other silvicultural practices during the southern USA lumber boom circa 1900 (AL Historical Commission, 2002; Fickle, 2014). This property was purchased by the Weyerhaeuser Company and has been used for both rotational pine harvest and forest biofuel research from 2010-2016 (Chescheir et al., 2018; Dobbs, 2016). The watershed is located within the larger Fall Line Hills level IV ecoregion,

and therefore has a historic forest structure of mixed coniferous and deciduous species (primarily oaks, hickory, and pines, with some longleaf reintroduction efforts; Griffith et al., 2001).

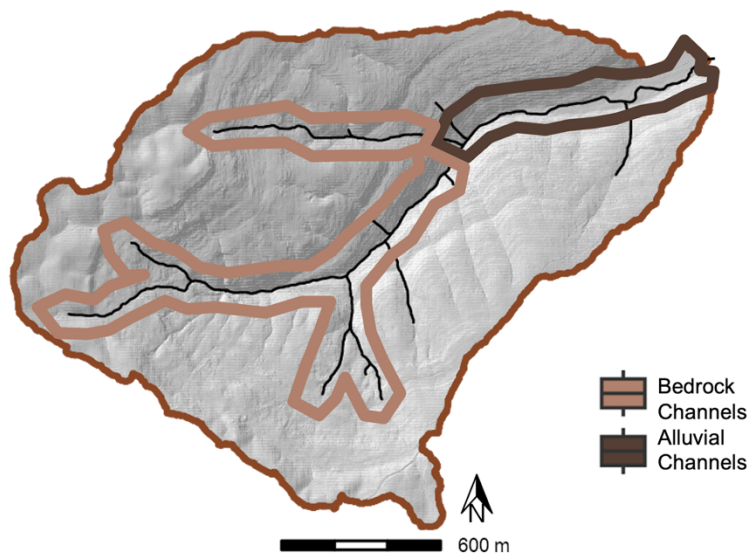


Figure S1. Hydrogeomorphic features of the instrumented portions of the Appalachian Plateaus watershed.

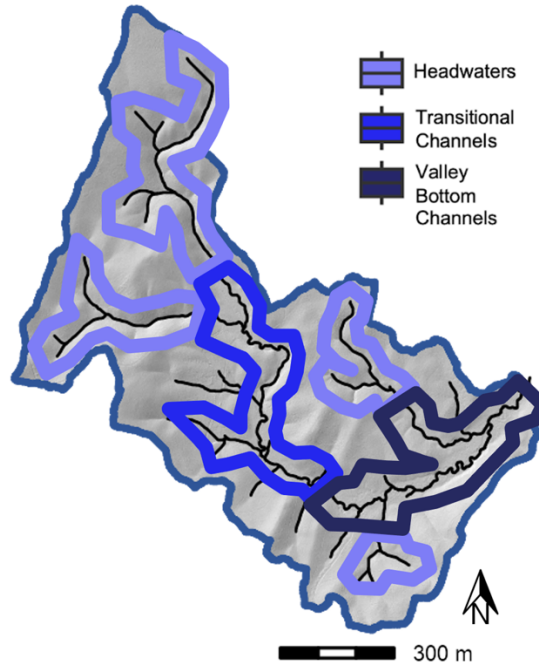


Figure S2. Hydrogeomorphic features of the instrumented portions of the Piedmont watershed.

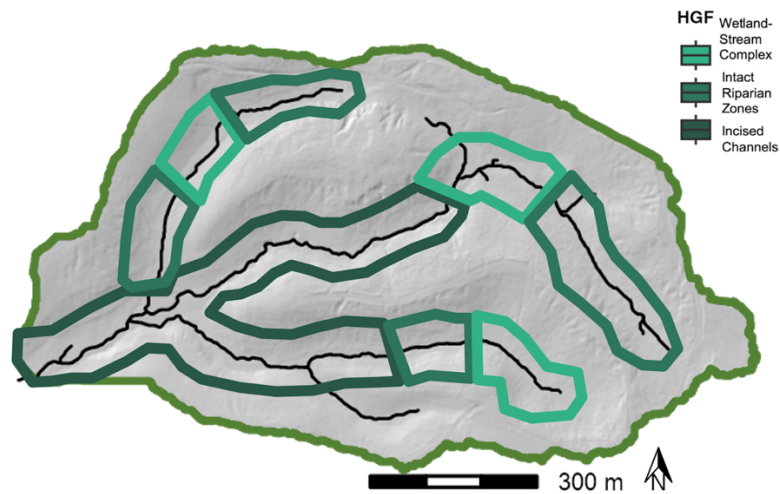


Figure S3. Hydrogeomorphic features of the instrumented portions of the Coastal Plain watershed.

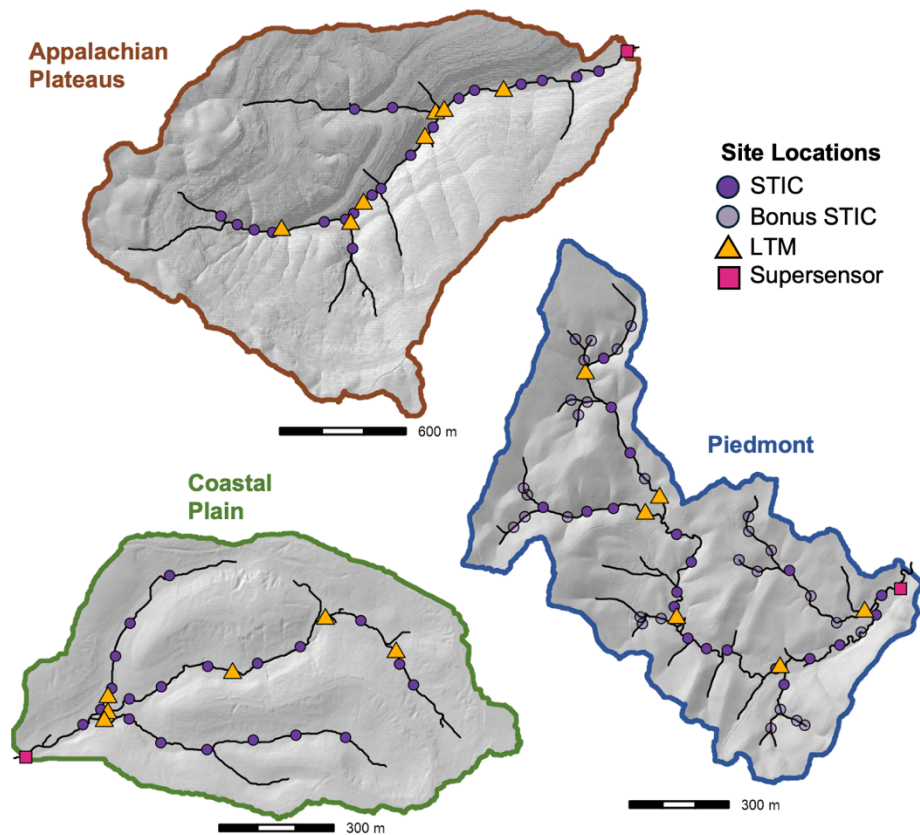


Figure S4. Sensor networks of the three research watersheds. Each watershed shows the three different types of sensors present (STIC = water presence/absence; Bonus STIC = the high-density additional sensors deployed in the Piedmont research watershed; LTM = Long-Term Monitoring locations, where stilling wells and piezometers were deployed in the channel and regular water sampling occurred; Supersensor = the outlet monitoring location, where water level and discharge were measured, as well as a high-frequency water quality sonde).

Table S1. T A description of all physiographic metrics calculated for this study.

Category	Metric	Scale	Description	Reference
Topographic	Slope	Site (1m)	Slope (%) extracted from the DEM at the sensor location using <i>wbt_slope()</i>	Lindsay, 2016; Florinsky, 2016
	Buffer slope	Site (5m)	Slope (%) averaged in a 5m circular buffer around the sensor location using <i>wbt_slope()</i>	sensu Warix et al., 2023; Lindsay, 2016
	Channel Slope	Reach (25m)	Slope (%) of only the channel network averaged across a 25m reach using <i>wbt_stream_slope_continuous()</i>	Lindsay, 2016
	Curvature	Site (1m)	Total curvature (m^{-1}) of the topographic surface using <i>wbt_total_curvature()</i>	Wilson, 2018; Lindsay, 2016
	Distance to outlet	Site	In-stream distance (m) from watershed outlet to sensor location using <i>wbt_distance_to_outlet()</i>	Lindsay, 2016
	Topographic Wetness Index (TWI)	Site (1m)	TWI of the sensor location calculated as $\ln(\text{catchment area} / \tan(\text{slope}))$ using <i>wbt_wetness_index()</i>	Beven & Kirkby, 1979; Lindsay, 2016
	Topographic Position Index (TPI)	Site (5m)	TPI of the 5m circular buffer around the sensor calculated as (focal elevation - mean(all other cell elevations)) using <i>TPI()</i>	llich et al., 2025
	Drainage density	Site	Upstream length (m) divided by drainage area of the sensor location	Montgomery & Dietrich, 1989; Godsey & Kirchner, 2014
	α , drainage density exponent	Network	The scaling exponent of the relationship between drainage area and distance downstream, calculated as length as a function of activation area threshold $^{-\alpha}$ ($L \propto A_{\alpha}^{-\alpha}$)	Prancevic & Kirchner, 2019
	θ , slope exponent	Network	The scaling exponent of the relationship between slope and drainage area, calculated as length as a function of drainage area $^{-\theta}$ ($S \propto A^{-\theta}$)	Prancevic & Kirchner, 2019
	δ , curvature coefficient	Network	The coefficient of the relationship between topographic curvature and drainage area, calculated as ($C = \delta \ln A + C_0$)	Prancevic & Kirchner, 2019
	β , network expansion exponent	Network	The exponent of the relationship between stream length and discharge at the outlet, calculated as ($L \propto Q_{\beta}$)	Godsey & Kirchner, 2014; Prancevic & Kirchner, 2019
γ , transmissivity exponent	Network	The scaling exponent of the theoretical relationship between transmissivity and drainage area, calculated as transmissivity as a function of drainage area $^{-\gamma}$ ($T \propto A^{-\gamma}$)	Prancevic & Kirchner, 2019	
Soil	Saturated hydraulic conductivity	HGF	Ability of saturated pores to transmit water ($\mu\text{m/s}$) in the upper 100 cm of the soil profile for	Soil Survey Staff, 2025

			each soil map unit, derived from soil structure, porosity, and texture data	
	Percent sand	HGF	Sand textural content (%) in the total soil profile as a weighted average for each soil map unit	Soil Survey Staff, 2025
	Percent silt	HGF	Silt textural content (%) in the total soil profile as a weighted average for each soil map unit	Soil Survey Staff, 2025
	Percent clay	HGF	Clay textural content (%) in the total soil profile as a weighted average for each soil map unit	Soil Survey Staff, 2025
	Organic matter content	HGF	Organic matter (%) by weight in the upper 50 cm of the soil profile for each soil map unit	Soil Survey Staff, 2025
Geology	Primary lithologic unit	HGF	Most surficial geologic layer; identified as parent material from soil surveys for each soil map unit	Soil Survey Staff, 2025; Szabo et al., 1988
	Depth to bedrock	HGF	Average depth (cm) to a lithologic restrictive layer for each soil map unit	Soil Survey Staff, 2025
Vegetation	Percent coniferous vegetation	HGF	Relative percentage of coniferous vegetation (%), derived from the difference between leaf off and leaf on densiometer measurements	

Table S2. All topographic coefficients calculated for the study.

Watershed	Predicted expansion exponent, β	Observed expansion exponent, β	Drainage density exponent, α	Slope exponent, θ	Transmissivity exponent, γ	Curvature coefficient, δ
Appalachian Plateau (Burks Creek)	0.0835	0.128	0.586	0.453	3.13	4.05
Piedmont (Pendergrass Creek)	-0.12	0.039	0.418	0.405	9.31	-2.84
Coastal Plain (Shambley Creek)	0.485	0.103	0.156	0.271	0.244	-0.293
Providence Creek ^a	0.34	0.401	0.576	0.02	0.42	0.74
Bull Creek ^a	0.14	0.182	0.399	0.165	1.03	1.37
Caspar Creek ^a	0.277	0.31	0.469	0.726	-0.21	0.3
Sagehen Creek ^a	0.3	0.312	0.419	0.284	0.06	0.39
McDonald 1 ^b	0.095	0.058	0.484	0.487	2.95	2.59
McDonald 2 ^b	0.062	0.109	0.675	0.081	10.56	6.49
Elder Creek ^c	0.219	0.175	0.487	0.402	1.38	0.83
Cougar Creek ^d	0.098	0.083	0.379	0.238	3.33	1.96
Dunce Creek ^d	0.086	0.093	0.442	0.126	3.63	2.81
Goat Creek ^d	0.112	0.055	0.245	0.257	3.19	0.9
Pioneer Creek ^d	0.24	0.197	0.595	0.339	1.68	1.03
Yellow Barn ^e	0.168	0.114	0.49	0.273	3.02	1.35
Coweeta 40 ^f	-0.14	0.04	0.384	0.39	8.21	-2.32
Fernow 37 ^f	0.195	0.18	0.593	0.173	2.12	1.49
Hubbard 25 ^f	0.15	0.59	0.28	0.076	-0.6	0.81
Hubbard 42 ^f	0.166	0.24	0.578	0.128	1.28	1.79
S. Fork Potts 70 ^f	0.089	0.14	0.542	0.393	2.48	3.26

Note: All variables retrieved from Prancevic & Kirchner (2019)

^aOriginally from Godsey & Kirchner (2014)^bOriginally from Roberts & Klingeman (1972)^cOriginally from Lovill et al. (2018)^dOriginally from Whiting & Godsey (2016)^eOriginally from Shaw (2016)^fOriginally from Jensen et al. (2017)**Table S3.** All topographic coefficients calculated for the study.

Data	Model	R²	RMSE	MAE	MAPE
Test	Coastal Plain	0.56	0.07	0.05	9.6
	Piedmont	0.75	0.15	0.12	18.5
	Appalachian Plateaus	0.16	0.24	0.21	42.6
	<i>Global</i>	<i>0.10</i>	<i>0.23</i>	<i>0.18</i>	<i>42.7</i>
Train	Coastal Plain	0.92	0.09	0.07	30.8
	Piedmont	0.92	0.08	0.06	11.9
	Appalachian Plateaus	0.88	0.10	0.08	23.5
	<i>Global</i>	<i>0.95</i>	<i>0.09</i>	<i>0.07</i>	<i>23.7</i>

Note: models were evaluated using Root Mean Squared Error (RMSE), coefficient of determination (R²), Mean Absolute Error (MAE), and Mean Absolute Percent Error (MAPE)

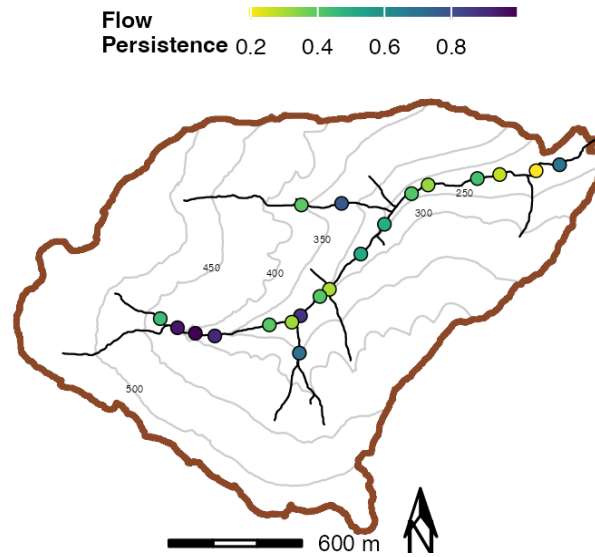


Figure S5. The Appalachian Plateaus watershed, with each site colored by surface water persistence over the 2022-2024 water years.

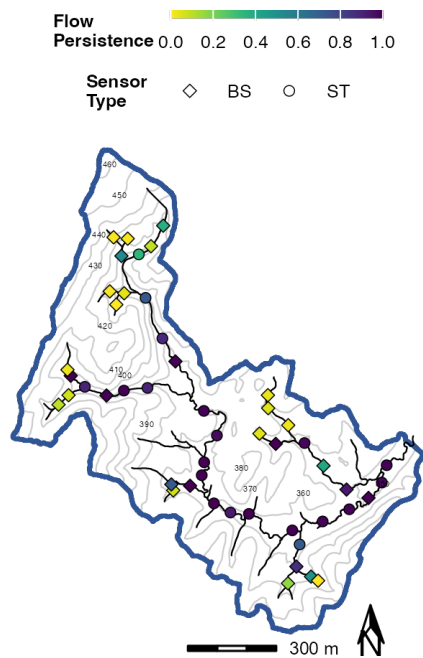


Figure S6. The Piedmont research watershed, with each site colored by water persistence over the period of record. Permanent sensors ($n = 20$) are indicated by circles, and measured water persistence over the 2022-2024 water years. The additional high-density network sensors ($n = 29$) are indicated by diamonds, and recorded water persistence from May 2022 through April 2023.

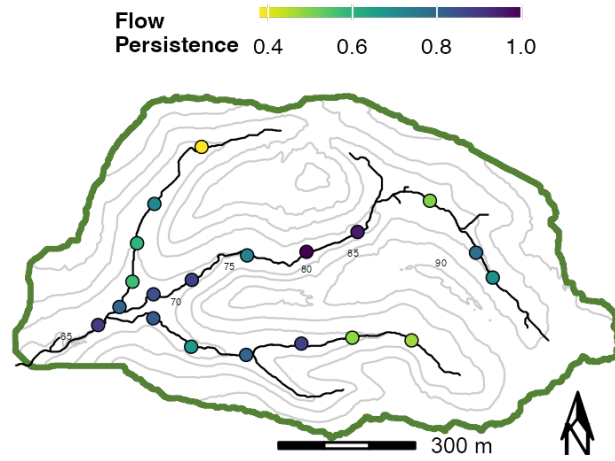


Figure S7. The Coastal Plain research watershed, with each site colored by water persistence over the 2022-2024 water years.